CANADIAN THESES ON MICROFICHE

THÈSES CANADIENNES SUR MICROFICHE

National Library of Canada
Collections Development Branch

Canadian Theses on
Microfiche Service

Ottawa, Canada
K1A 0N4

Bibliothèque nationale du Canada
Direction du développement des collections

Service des thèses canadiennes
sur microfiche

NOTICE

The quality of this microfiche is heavily dependent upon the quality of the original thesis submitted for microfilming. Every effort has been made to ensure the highest quality of reproduction possible.

If pages are missing, contact the university which granted the degree.

Some pages may have indistinct print especially if the original pages were typed with a poor typewriter ribbon or if the university sent us an inferior photocopy.

Previously copyrighted materials (journal articles, published tests, etc.) are not filmed.

Reproduction in full or in part of this film is governed by the Canadian Copyright Act, R.S.C. 1970, c. C-30. Please read the authorization forms which accompany this thesis.

AVIS

La qualité de cette microfiche dépend grandement de la qualité de la thèse soumise au microfilmage. Nous avons tout fait pour assurer une qualité supérieure de reproduction.

S'il manque des pages, veuillez communiquer avec l'université qui a conféré le grade.

La qualité d'impression de certaines pages peut laisser à désirer, surtout si les pages originales ont été dactylographiées à l'aide d'un ruban usé ou si l'université nous a fait parvenir une photocopie de qualité inférieure.

Les documents qui font déjà l'objet d'un droit d'auteur (articles de revue, examens publiés, etc.) ne sont pas microfilmés.

La reproduction, même partielle, de ce microfilm est soumise à la Loi canadienne sur le droit d'auteur, SRC 1970, c. C-30. Veuillez prendre connaissance des formules d'autorisation qui accompagnent cette thèse.

THIS DISSERTATION
HAS BEEN MICROFILMED
EXACTLY AS RECEIVED

LA THÈSE A ÉTÉ
MICROFILMÉE TELLE QUE
NOUS L'AVONS REÇUE

Canada

NL 339 (r. 88/09)

National Library of Canada
Bibliothèque nationale du Canada

Ottawa, Canada
K1A 0N4

19

TC –

ISBN 0-315-21215-2

CANADIAN THESES ON MICROFICHE SERVICE – SERVICE DES THÈSES CANADIENNES SUR MICROFICHE

PERMISION TO MICROFILM – AUTORISATION DE MICROFILMER

• Please print or type – Écrire en lettres moulées ou dactylographier

AUTHOR – AUTEUR

Full Name of Author – Nom complet de l'auteur

GARY KAM WING LIN

Date of Birth – Date de naissance

January 3rd, ~~59~~ 1959

Canadian Citizen – Citoyen canadien

☐ Yes / Oui ☑ No / Non

Country of Birth – Lieu de naissance

HONG KONG (British)

Permanent Address – Résidence fixe

284, YU CHAU ST.,
4th FLOOR, SHAM SHUI PO.,
KOWLOON, HONG KONG.

THESIS – THÈSE

Title of Thesis – Titre de la thèse

Fault Location Using Least Squares Estimation

Degree for which thesis was presented
Grade pour lequel cette thèse fut présentée

M.Sc.

Year this degree conferred
Année d'obtention de ce grade

1985

University – Université

Alberta

Name of Supervisor – Nom du directeur de thèse

K.E. BOLLINGER

AUTHORIZATION – AUTORISATION

Permission is hereby granted to the NATIONAL LIBRARY OF CANADA to **microfilm** this thesis and to **lend** or **sell copies of the film.**

The author reserves other publication rights, and neither the thesis nor extensive extracts from it may be printed or otherwise reproduced without the author's written permission.

L'autorisation est, par la présente, accordée à la BIBLIOTHÈQUE NATIONALE DU CANADA de **microfilmer** cette thèse et de **prêter** ou de **vendre des exemplaires du film.**

L'auteur se réserve les autres droits de publication; ni la thèse ni de longs extraits de celle-ci ne doivent être imprimés ou autrement reproduits sans l'autorisation écrite de l'auteur.

ATTACH FORM TO THESIS – VEUILLEZ JOINDRE CE FORMULAIRE À LA THÈSE

Signature

Gary Lin

Date

JAN 30th, 85

NL-91 (r. 84/03)

Canada

THE UNIVERSITY OF ALBERTA

Fault Location Using Least Squares Estimation

by

(C) Gary Kam Wing Lin

A THESIS

SUBMITTED TO THE FACULTY OF GRADUATE STUDIES AND RESEARCH

IN PARTIAL FULFILMENT OF THE REQUIREMENTS FOR THE DEGREE

OF Master of Science

Department of Electrical Engineering

EDMONTON, ALBERTA

Spring 1985

THE UNIVERSITY OF ALBERTA

RELEASE FORM

NAME OF AUTHOR Gary Kam Wing Lin

TITLE OF THESIS Fault Location Using Least Squares Estimation

DEGREE FOR WHICH THESIS WAS PRESENTED Master of Science

YEAR THIS DEGREE GRANTED Spring 1985

Permission is hereby granted to THE UNIVERSITY OF ALBERTA LIBRARY to reproduce single copies of this thesis and to lend or sell such copies for private, scholarly or scientific research purposes only.

The author reserves other publication rights, and neither the thesis nor extensive extracts from it may be printed or otherwise reproduced without the author's written permission.

(SIGNED) Gary Lin

PERMANENT ADDRESS:

284 YU CHAU ST.

4TH FLOOR, SHAM SHUI PO

KOWLOON, HONG KONG

DATED JAN. 30 1985

THE UNIVERSITY OF ALBERTA

FACULTY OF GRADUATE STUDIES AND RESEARCH

The undersigned certify that they have read, and recommend to the Faculty of Graduate Studies and Research, for acceptance, a thesis entitled Fault Location Using Least Squares Estimation submitted by Gary Kam Wing Lin in partial fulfilment of the requirements for the degree of Master of Science.

...D.C. Bellinger...

Supervisor

...R. E. Rink...

...M. Sachdev...

...Nirdosh...

Date...Jan. 30, 1985.....

Abstract

An iterative algorithm based on least squares estimation theory is proposed to determine the fault location of transmission lines. The required input data are the voltages and currents at the local end only. The estimation algorithm, put forward in this study, does not require filtering of the fault data and hence yields a technique that is quite efficient.

Several different simulation studies were analyzed for different types of fault in order to examine the merits of this algorithm.

ACKNOWLEDGEMENTS

I wish to thank my supervisor, Prof. K. E. Bollinger, for his invaluable guidance on this thesis.

Helpful discussions with Dr. R. E. Rink and Dr. V. G. Gourishanker are gratefully appreciated.

I would like to thank Mr. Philip Wood and Mr. Joey Siu for their helpful suggestions and comments to this thesis.

I would also like to thank Mr. Steve Au for his encouragement and suggestions.

Financial support from the Department of Electrical Engineering is gratefully acknowledged.

Table of Contents

Chapter		Page
1.	Introduction	1
	1.1 Contribution of Fault Locator to Power System	1
	1.2 Review of Past Works	2
	1.3 Scope of Research	5
2.	Modelling for Real System	7
	2.1 Overall System Model	7
	2.2 Fault-Caused Model : Superposition Principle	7
	2.3 Instantaneous Symmetrical Component	9
	2.4 Interconnection of Sequence Network to Represent a Single Line to Ground Fault	11
	2.5 Mathematical Formulation for the Model of a Single Line to Ground Fault	14
	2.6 Three Phase Fault	16
	2.7 Mathematical Formulation for the Model of a Three Phase Fault	17
3.	Fault Simulation (Real System)	19
	3.1 Simulated Line with R-L Representation	19
	3.1.1 Simulation of Fault	19
	3.2 Simulated Line with π Section Representation	21
	3.2.1 Simulation of Fault	21
	3.3 Determination of Step Size for Numerical Solution of the Transmission Line	23
4.	Background of Least Squares Estimation Theory	26
	4.1 Introduction	26
	4.2 Mathematical Formulation for the Least Squares Estimation Method	28
	4.3 Computational Aspect	32

5. Least Squares Estimator 36

5.1 Application to Fault Location for a Single Line to Ground Fault 36

5.2 Application to Fault Location for a Three Phase Fault 39

5.3 Discussion of Results 44

5.3.1 Effect of G on Estimator Convergence ...46

5.3.2 Effect of Changing Fault Distance on Location Accuracy 46

5.3.3 Effect of Changing Fault Resistance on Location Accuracy 47

5.3.4 Reconstruction of Waveform 48

5.3.5 Modelling Error 49

6. Conclusions 68

References 70

Appendix A1 : Circuit Parameters for a Transmission Line .74

Appendix A2 : Derivation of State Space Form for a R-L Series Transmission Line 75

Appendix A3 : Derivation of State Space Form for Eight Sections Transmission Line 80

Appendix A4 : Expression for Equation (5.7) 89

Appendix A5 : Expression for Equation (5.13) 90

Appendix A6 : Verification of the Presence of Mutual Coupling in the Phase Quantities 91

List of Tables

Table		Page
3.1	Eigenvalues of A with fault resistance of 0.12 p.u. (30Ω)	25
5.1	Description of systems and models used in different tests	45

List of Figures

Figure		Page
2.1	Faulted system model	8
2.2	Prefault component	10
2.3	Fault-caused component	10
2.4	Sequence network connection for a single line to ground fault	13
2.5	Simplified sequence network	15
2.6	Network for a three phase fault	18
3.1	R-L series network	20
3.2	π section representation of transmission line	22
4.1	Least squares estimation system	27
4.2	Algorithm of parameter estimation	33
5.1	Algorithm of parameter estimation for single line to ground fault	40
5.2	Algorithm of parameter estimation for three-phase fault	43
5.3	Typical transient voltage of R-L transmission line	50
5.4	Typical transient current of R-L transmission line	51
5.5	Typical transient voltage of π section transmission line	52
5.6	Typical transient current of π section transmission line	53
5.7	Effect of G on algorithm, with g_{11} = 2.0	54
5.8	Effect of G on algorithm, with g_{11} = 0.4	55
5.9	Estimated distance versus data window with actual fault distance of 25 miles and fault resistance of 0.12 p.u	56

5.10 Estimated distance versus data window with actual fault distance of 50 miles and fault resistance of 0.12 p.u.....57

5.11 Estimated distance versus data window with actual fault distance of 75 miles and fault resistance of 0.12 p.u.....58

5.12 Estimated distance versus data window with actual fault distance of 50 miles and fault resistance of 0.004 p.u.....59

5.13 Output waveform from test 1 with initial estimates..60

5.14 Output waveform from test 1 with identified parameters.....61

5.15 Output waveform from test 2 with initial estimates..62

5.16 Output waveform from test 2 with identified parameters.....63

5.17 Output waveform from test 3 with initial estimates (positive sequence current).....64

5.18 Output waveform from test 3 with identified parameters (positive sequence current)...65

5.19 Output waveform from test 3 with initial estimates (zero sequence current).....66

5.20 Output waveform from test 3 with identified parameters (zero sequence current).....67

List of Abbreviations and Symbols

Abbreviations

KV	- kilovolt
MVA	- megavoltampere

Symbols

$v_s(t)$	- instantaneous source voltage
$v_r(t)$	- instantaneous remote end voltage
$Z_s(p)$	- operational impedance of source end
$Z_r(p)$	- operational impedance of remote end
p	- differential operator
$Z(p)$	- operational impedance per mile
R_f	- fault resistance
$v(t)$	- instantaneous voltage
$v_p(t)$	- prefault instantaneous voltage
$\Delta v(t)$	- instantaneous fault caused voltage
$i(t)$	- instantaneous current
$i_p(t)$	- prefault instantaneous current
$\Delta i(t)$	- instantaneous fault caused current
d_o	- total length of a transmission line
d	- distance of fault from measurement point
v_f	- prefault voltage at fault point
i_f	- fault current
v_o	- instantaneous zero sequence voltage (fault caused component)

v_1 - instantaneous positive sequence voltage (fault caused component)

i_0 - instantaneous zero sequence current (fault caused component)

i_1 - instantaneous positive sequence current (fault caused component)

$\dot{i}_0$ - derivative of i_0

$\dot{i}_1$ - derivative of i_1

$\dot{i}_f$ - derivative of fault current

R_0 - zero sequence line resistance/mile

R_{r0} - zero sequence Thevenin resistance

R_1 - positive sequence line resistance/mile

R_{r1} - positive sequence Thevenin resistance

L_0 - zero sequence line inductance/mile

L_{r0} - zero sequence Thevenin inductance

L_1 - positive sequence line inductance/mile

L_{r1} - positive sequence Thevenin inductance

v_a - instantaneous voltage of phase 'a' at measurement point (fault caused component)

i_a - instantaneous current of phase 'a' at measurement point (fault caused component)

$\dot{i}_a$ - derivative of i_a

$\bar{V}_a$ - steady state value of v_a (complex quantity)

$\bar{V}_f$ - steady state value of v_f (complex quantity)

$|\bar{V}_f|$ - magnitude of phasor $\bar{V}_f$

$\bar{I}_a$ - steady state value of i_a (complex quantity)

θ_f - phase angle of vector $\bar{V}_f$

C_1	- capacitance at measurement point or at remote end
C_2	- capacitance in between π section
X	- state vector of model
Y	- output vector from model
U	- input vector to model or real system
$A(\alpha)$	- state coefficient matrix
$B(\alpha)$	- input coefficient matrix
$C(\alpha)$	- output coefficient matrix
α	- parameter vector
J	- cost function
Y_r	- output from real system
W	- weighting matrix
t_0	- initial observation time
t_k	- final observation time
t_f	- fault inception time
α_0	- initial estimated parameter vector
$\hat{\alpha}$	- true value of parameter vector
$\sqrt{}$	- square root
e	- error signal

Superscripts

T	- transpose of matrix

CHAPTER I

Introduction

1.1 Contribution of Fault Locator to Power System

Transmission lines are a critical segment of a power system. Unfortunately, faults on transmission lines are unavoidable and thus provision for protecting the lines must be used. Faults may be due to lightning, inadvertent conductor grounding causing short-circuited and localized impairment of insulation, etc. The fault may result in damage to generators, lines, or transformers if not removed quickly. Fortunately, this damage is kept within limits due to short clearing times of modern line protection equipment.

Following a fault on the system, action is initiated to correct the fault. A valuable asset to the operation of the power system is to be able to locate the fault so that the necessary repairs can be carried out to put the line back into service without undue delay. A fault locator situated at a local end can determine a fault quickly compared with the time-consuming method of visual inspection [1]. An automatic fault locator is a much better choice if access is hindered by floods, slides or storms and rough terrain. As power systems expand, the need for reliable and accurate fault location techniques has become more evident.

1.2 Review of Past Works

An analog fault locator was developed to locate every fault in the event of a short circuit [2]. The distance to the fault was determined by means of impedance measurements. In order to prevent impairment of the measurement by noise voltages of higher frequencies, suitable filters were required. For this locator, distance can be determined directly if the line has a uniform impedance per kilometer over its entire length. Otherwise, evaluation is best made with the aid of a table. With the evolution of solid state devices, a handy, compact transistorised fault locator was developed [3]. It was designed for unarmoured power cables widely employed in the mining industries. The operation of this locator is based on the principle of electro-magnetic induction. There are some disadvantages for this device. Firstly, the load has to be disconnected to determine the location of the fault. Secondly, if the cable is too long, it may take a long time to locate the fault. Despite these disadvantages, this locator is really an applicable device for mining industries.

Existing transmission line fault location methods based on measured quantities at one or more points on the line may be broadly classified into two categories. The first method is based on distributed parameter line model in which the fault location is deduced by analyzing voltage and current travelling wave measurements. Vitins [4] presented a

correlation method for transmission line protection. He suggested that the transient phenomena initiated by the occurrence of a fault on a power transmission line be described by the telegraph equation. It was shown that the fault distance appeared as a time delay between the instantaneous value of the forward travelling wave and the backward travelling wave at the measurement site. Filtering is a necessary step for this method. Although Kohlas [5] used the telegraph equation to represent a line model (as Vitins did), he approached the problem differently. In his method, a voltage profile is used to estimate the location of the fault. The complexity and accuracy of the above two methods mainly depend on the extent of simplifications of the overall system configuration. The second method, often used in transmission line protection, is based on lumped parameter line model where the objective is to find a complex impedance of the system in the direction of the fault as seen from the measurement site, after which fault distance is to be deduced. Different algorithms were developed to determine the impedance accurately. One algorithm suggested by Brooks [6] used least squares estimation method, with the assumption that the voltage and current waveforms contain at most a constant plus a fundamental harmonic. In general, the distorted waveforms, after the occurrence of a fault, contain a decaying d.c. component and components of the fundamental plus higher harmonic frequencies. Sachdev and Baribeau [7] took these

transient phenomena into account and came up with a different algorithm to calculate impedance. Another similar approach was presented by Smolinski [8]. Smolinski's algorithm does not require prior filtering of transmission line voltage and current signals to remove either transient d.c. offset component or transient high frequency components before calculating the impedance of the line. Since the above three methods mainly calculate the impedance for a faulted transmission line, one further step is required to locate the fault. Takagi, Yamakoski, Baba, Uemura and Sakaguchi [9] presented a fault location algorithm based on the Fourier analysis of a faulted network. Unfortunately, the assumption of lossless circuit elements and the requirement of digital filtering make this method not an attractive one. The bulky conventional equipment that is used in locating faults poses a problem due to limited space in a substation. This problem was solved by the use of digital fault locators [10]. Again, the filtering of undesirable higher harmonics in the output is required.

For most of the methods described above, the prior knowledge of fault resistance and the filtering of transient components are required. In order to solve this problem, Richards and Tan [11] presented a different approach to fault location. They treated the fault location problem as a parameter estimation problem of a dynamic system in which the response of the physical system was compared with that of the lumped parameter model. The model's parameters are

varied until an adequate match is obtained with the physical system response.

1.3 Scope of Research

Among the approaches mentioned above, the method suggested by Richards and Tan [11] is the best. This algorithm can be applied directly to recorded fault data immediately without prior knowledge of the fault resistance and the filtering process. In order to better understand how this concept operates, investigations and some simulations have been done for various system configurations. Although in [11] the circuit parameters for a transmission line are given, their paper does not mention the mathematical formulation of the line. Hence, one of the chapters in this thesis is devoted to this aspect.

The studies can basically be divided into two parts. The first part deals with simulating transimission lines (real system), from which the transient fault data are obtained. The second part is concerned with the fault location algorithm, where the fault data obtained from real system were fed into the algorithm in order to deduce the location of fault. A single line to ground fault on phase 'a' of a transmission line and symmetrical three phase fault were studied. Furthermore, the effects of changing fault resistance and fault location on the accuracy of estimation were examined.

Different models for the real system and their mathematical formulations are presented in Chapter Two. Chapter Three deals with the formulations of simulated transmission line. Two kinds of simulated line are presented. One is the simplified series resistance and inductance (R-L) representation and the other is the usual π section representation. Their state space equations and procedures to simulate a fault are also included.

A brief review of least squares theory and discussion on its computational aspect are presented in Chapter Four. The application of least squares to the problem of fault location and various simulation results are contained in Chapter Five.

CHAPTER II

Modelling for Real System

2.1 Overall System Model

The model used here is shown in Figure 2.1 [11], where both ends of the transmission line are represented by three phase Thevenin equivalents for transients. It is a double-end feed transmission line with V_s at the source end of $1.0*\cos(377*t+5°)$ p.u., and V_r at the remote end of $1.0*\cos(377*t)$ p.u.. These voltages are chosen arbitrarily. $Z_s(p)$ and $Z_r(p)$ are the operational impedances ($p=d/dt$) of the Thevenin equivalents at the measurement and remote ends of the line respectively, $Z(p) = R+Lp$ and R_f are the operational impedance per mile and the fault resistance respectively, and d_o is the total line length.

2.2 Fault-Caused Model : Superposition Principle

The inception of a fault in a power system will cause the postfault voltage v and current i at the measurement point to deviate from the steady state prefault voltage v_p and current i_p, respectively. Hence

$$v(t) = v_p(t) + \Delta v(t)$$

$$i(t) = i_p(t) + \Delta i(t) \qquad (2.1)$$

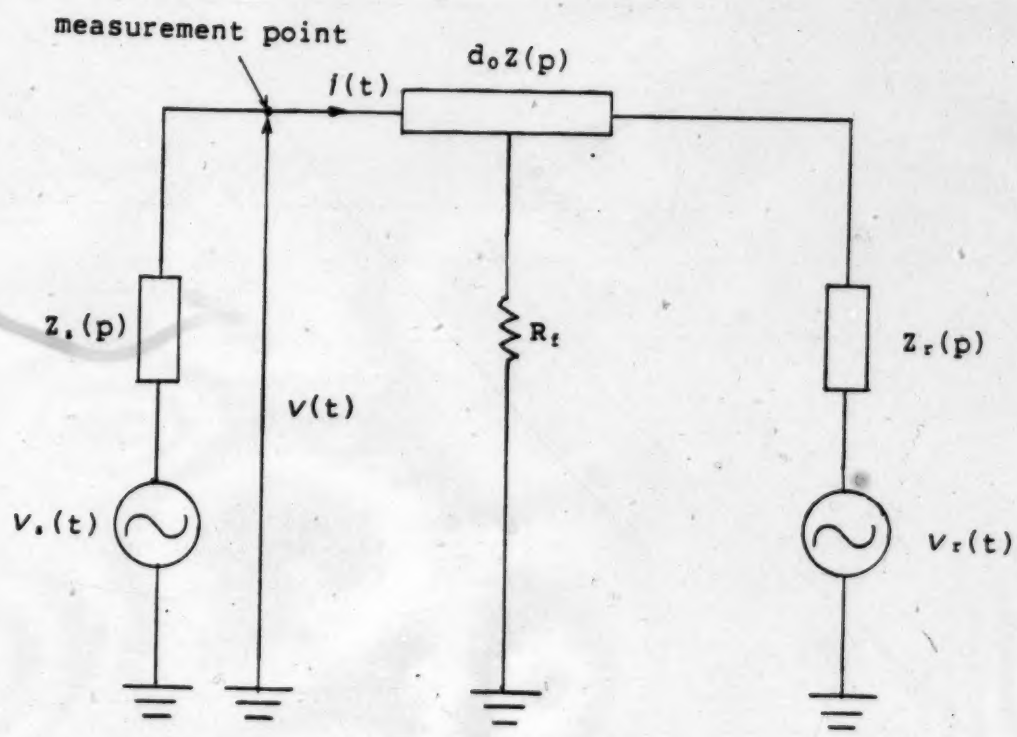

Figure 2.1 Faulted system model

where $\Delta v(t)$ and $\Delta i(t)$ denote the fault caused voltage and current deviations as functions of time. The deviation signals can be considered to be generated by putting a fictitious voltage source at the fault point F with a voltage equal in magnitude and opposite in sign to the prefault voltage at the fault point. The superposition of the resulting deviation signals and the prefault waveforms yield the postfault waveforms. Based on this principle, Figure 2.1 can be decomposed into Figure 2.2 of prefault components and Figure 2.3 of fault-caused components. Note that v_f is the prefault voltage at fault point F, and the fault is assumed to occur at a distance of d from the measurement point.

2.3 Instantaneous Symmetrical Component

The line fault is generally asymmetrical, except for the case of a three phase symmetrical fault. Instead of dealing with this asymmetrical condition, symmetrical component transformation will produce three symmetrical networks. It is noted that the transformation is a steady state concept. However, instantaneous values of subtransient voltages and currents in the immediate fault time period must be used for the parameter estimator. The transformation can be applied to instantaneous variables [12] [13] and the instantaneous symmetrical components are, in general, complex quantities. Moreover, the resulting instantaneous positive and negative sequence variables are generally

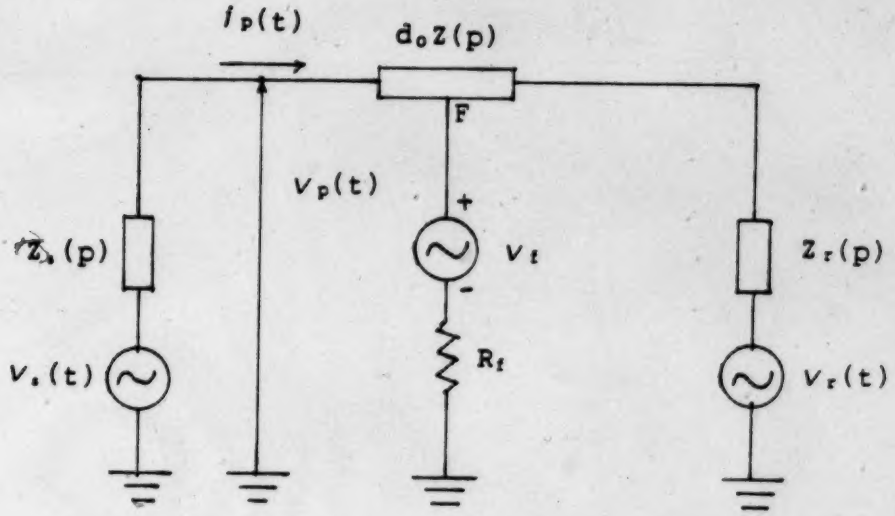

Figure 2.2 Prefault component

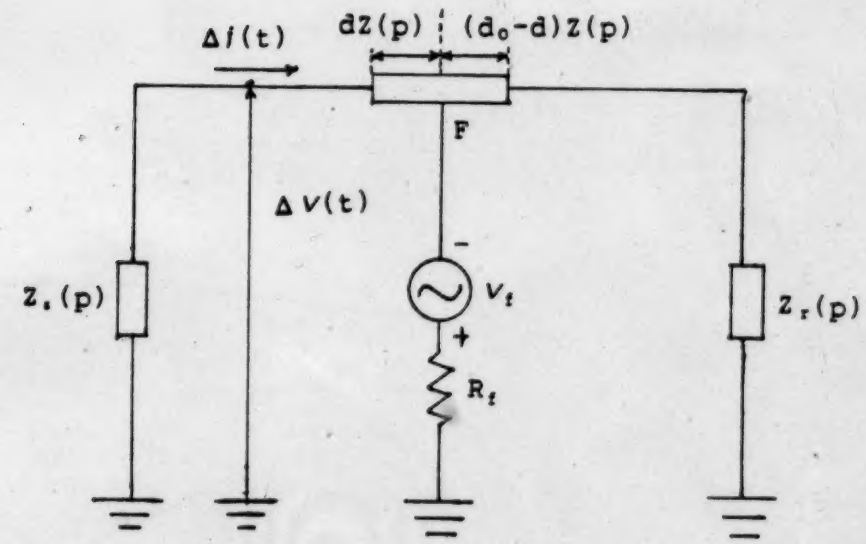

Figure 2.3 Fault-caused component

complex conjugate pairs. The inverse symmetrical component (power invariant) transformation maps the a,b,c voltages and currents into instantaneous complex 0,1,2 variables:

$$\Gamma_{012} = A^{-1}\Gamma_{abc} \tag{2.2}$$

where Γ may be voltages or currents and A^{-1} is equal to :

$$A^{-1} = \frac{1}{\sqrt{3}} \begin{bmatrix} 1 & 1 & 1 \\ 1 & a & a^2 \\ 1 & a^2 & a \end{bmatrix} \tag{2.3}$$

where $a = e^{j2\pi/3}$ (2.4)

2.4 Interconnection of Sequence Network to Represent a Single Line to Ground Fault

In order to obtain the sequence networks for the model, the following assumptions have been made :

1. The transmission line has frequency independent zero, positive and negative sequence impedances and the value of positive and negative sequences are equal.
2. The positive sequence inductance and the negative

sequence inductance are equal for the synchronous generator.

3. For the loading of induction motor, the positive and negative inductances are equal to the subtransient inductance, L", if the motor has a double cage or deep-bar rotor, and to the transient inductance L', if it has a single equivalent rotor winding.

Due to the above assumptions, the positive and negative sequences of the Thevenin equivalent at each end of the line are equal. If a single line to ground fault occurs on phase 'a' at distance d from the measurement point, the sequence network are connected as shown in Figure 2.4

For the sake of simplicity, the Thevenin equivalent operational impedance at the remote end of the line consists of a single equivalent resistance R_{rk} and inductance L_{rk}, k = 0,1. In this analysis, only the real parts of the instantaneous complex 0,1,2 variables are considered. Since positive and negative sequence voltages are complex conjugates, their imaginary parts will be cancelled. In other words, the imaginary parts are exact opposites and will not contribute any fault current. Also, the positive and negative sequence operational impedances for the transmission line are assumed equal. Hence, the positive and negative sequence networks are identical and are connected in series. Besides, the Thevenin equivalent operational impedance at the source end can be ignored because in the

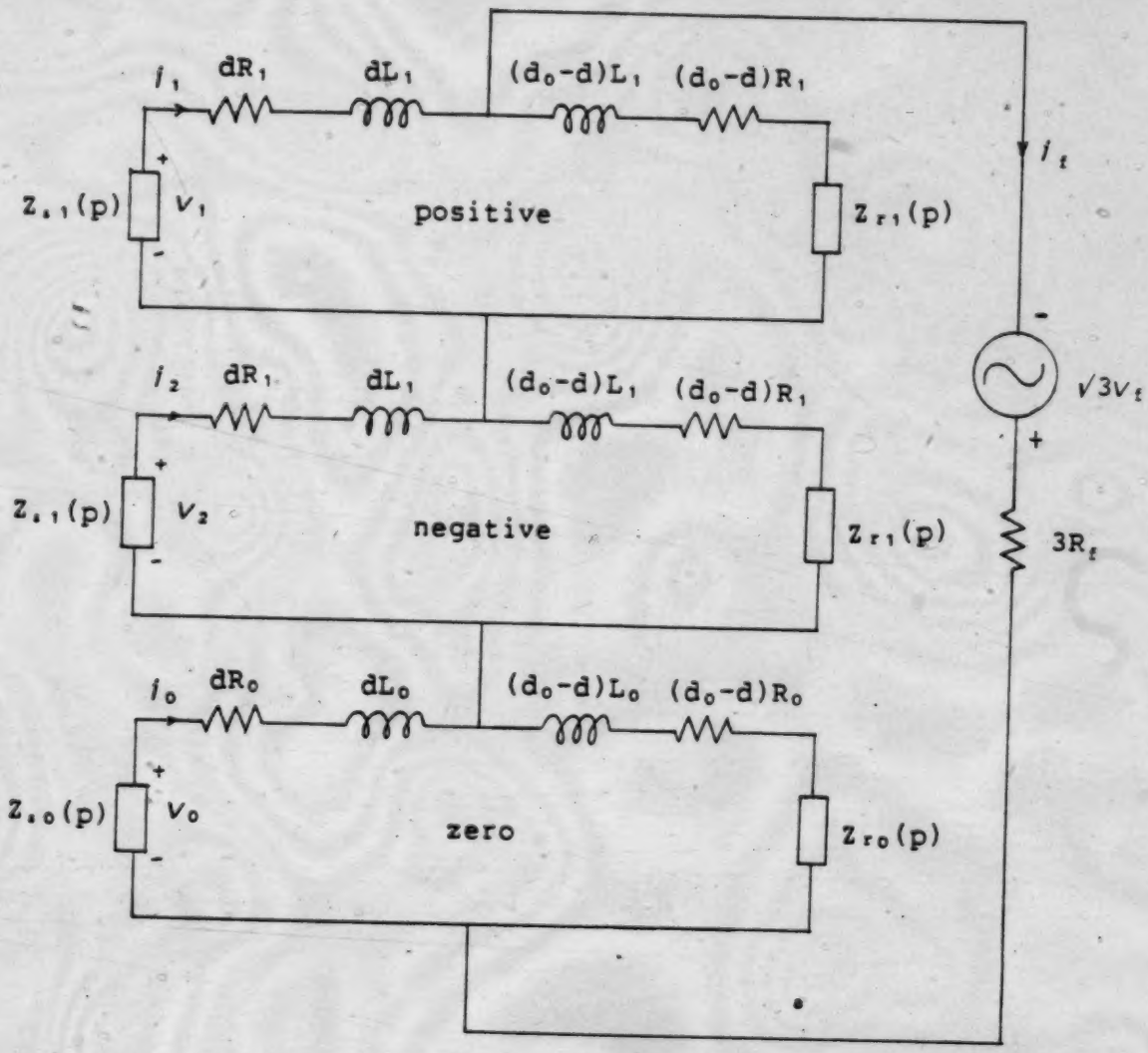

Figure 2.4 Sequence network connection for a single line to ground fault

fault location algorithm only the sequence voltages at the measurement point are required. Thus Figure 2.4 can be reduced to Figure 2.5.

2.5 Mathematical Formulation for the Model of a Single Line to Ground Fault

Applying Kirchhoff's voltage law to Figure 2.5 yields the following equations :

$$
\begin{aligned}
v_0 &= (d_0R_0+R_{r0})i_0 - [(d_0-d)R_0+R_{r0}]i_f \\
&\quad + (d_0L_0+L_{r0})\dot{i}_0 - [(d_0-d)L_0+L_{r0}]\dot{i}_f \\
2v_1 &= (2d_0R_1+2R_{r1})i_1 - [2(d_0-d)R_1+2R_{r1}]i_f \\
&\quad + (2d_0L_1+2L_{r1})\dot{i}_1 - [2(d_0-d)L_1+2L_{r1}]\dot{i}_f \qquad (2.5) \\
\sqrt{3}v_f &= -[(d_0-d)R_0+R_{r0}]i_0 - [2(d_0-d)R_1+2R_{r1}]i_1 \\
&\quad + [(d_0-d)(R_0+2R_1)+R_{r0}+2R_{r1}+3R_f]i_f \\
&\quad - [(d_0-d)L_0+L_{r0}]\dot{i}_0 - [2(d_0-d)L_1+2L_{r1}]\dot{i}_1 \\
&\quad + [(d_0-d)(L_0+2L_1)+L_{r0}+2L_{r1}]\dot{i}_f
\end{aligned}
$$

In this equation and the following analysis, v_0, v_1 and i_0, i_1 represent the real parts of zero and positive

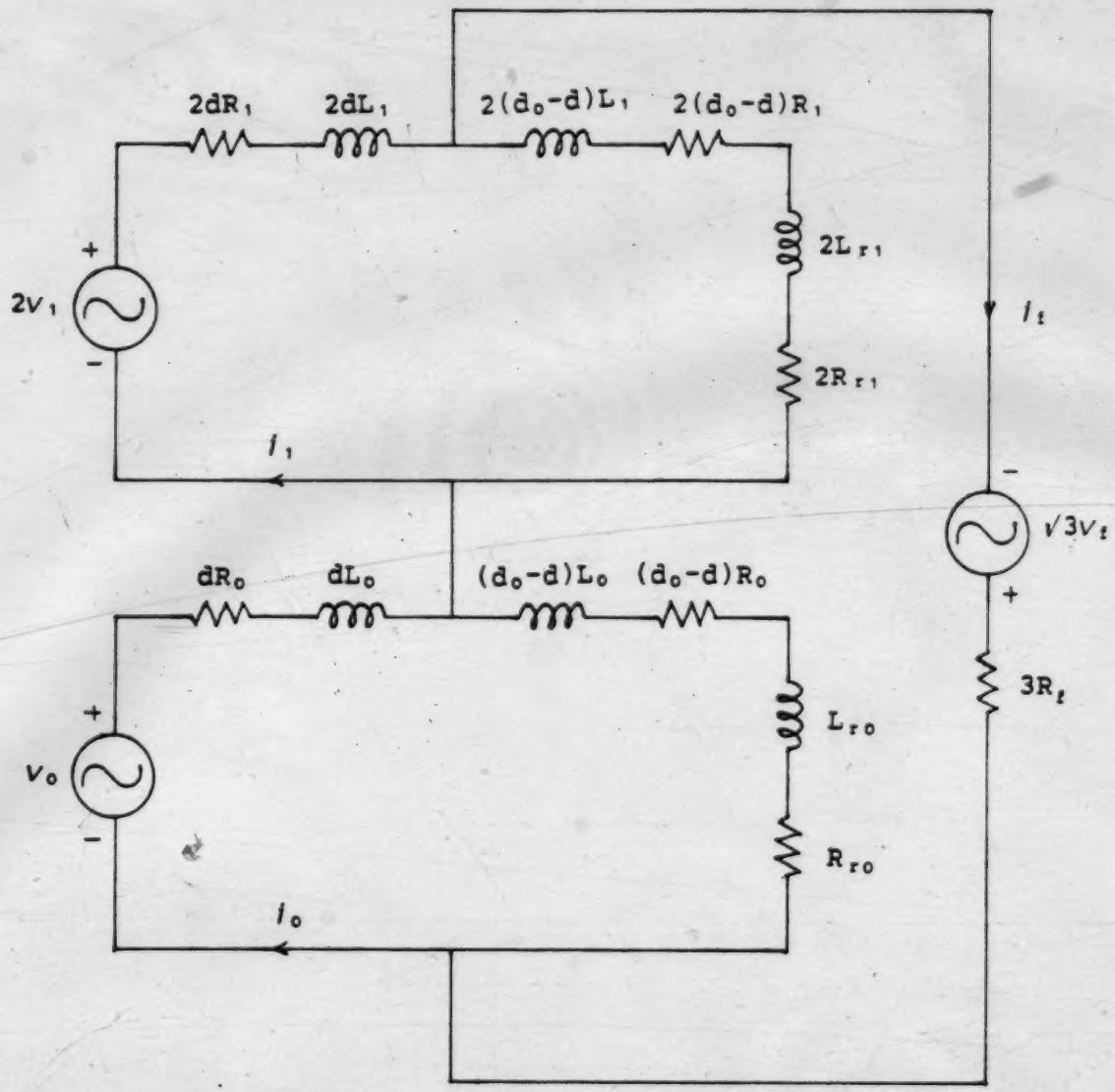

Figure 2.5 Simplified sequence network

sequence instantaneous fault-caused voltages and currents at the measurement point. i_f is the fault current through the fault resistance. v_f is the prefault sinusoidal voltage of phase 'a' at the fault point, which is a function of the prefault voltage and current at the measurement point, and the distance d. It can be expressed as :

$$\bar{V}_f = \bar{V}_a - d(R_1+j\omega_o L_1)\bar{I}_a \qquad (2.6)$$

$$v_f = \sqrt{2}*|\bar{V}_f|*\cos(\omega_o t+\theta_f) \qquad (2.7)$$

where $\bar{V}_f$, $\bar{V}_a$ and $\bar{I}_a$ are phasors. Note that v_f and θ_f are functions of $\bar{V}_a$, $\bar{I}_a$ and d. θ_f is the phase angle of vector $\bar{V}_f$. Whereas, $\bar{V}_a$ and $\bar{I}_a$ are prefault phasors at the measurement point.

2.6 Three Phase Fault

Any type of fault, if not cleared quickly, will develop into a three phase fault. Hence this type of fault is being investigated as well. As mentioned in section 2.3, this fault is a symmetrical one. In other words, phase a,b and c will retain their normal relative position. Hence symmetrical transformation is not necessary. The system model in section 2.1, the superposition principle and the assumptions in section 2.4 have to be used to develop a three phase fault model.

If a three phase fault occurs at distance d from the measurement point, the network can be drawn as in Figure 2.6.

2.7 Mathematical Formulation for the Model of a Three Phase Fault

Applying Kirchhoff's voltage law to Figure 2.6 yields the following equations :

$$v_a = (d_o R_1 + R_{r1}) i_a - [(d_o - d) R_1 + R_{r1}] i_f + (d_o L_1 + L_{r1}) \dot{i}_a - [(d_o - d) L_1 + L_{r1}] \dot{i}_f \qquad (2.8)$$

$$v_f = -[(d_o - d) R_1 + R_{r1}] i_a + [(d_o - d) R_1 + R_{r1} + R_f] i_f - [(d_o - d) L_1 + L_{r1}] \dot{i}_a + [(d_o - d) L_1 + L_{r1}] \dot{i}_f \qquad (2.9)$$

In these equations, v_a and i_a are the instantaneous fault-caused voltage and current respectively at the measurement point, and i_f is the fault current through the fault resistance. v_f is the prefault sinusoidal voltage of phase 'a' at the fault point, which is defined previously in equations (2.6) and (2.7). Note that phase 'a' is arbitrarily chosen as the reference phase. Voltages and currents in phases b and c can simply be found by applying phase rotations of -120° and +120° respectively to the phase 'a' quantities.

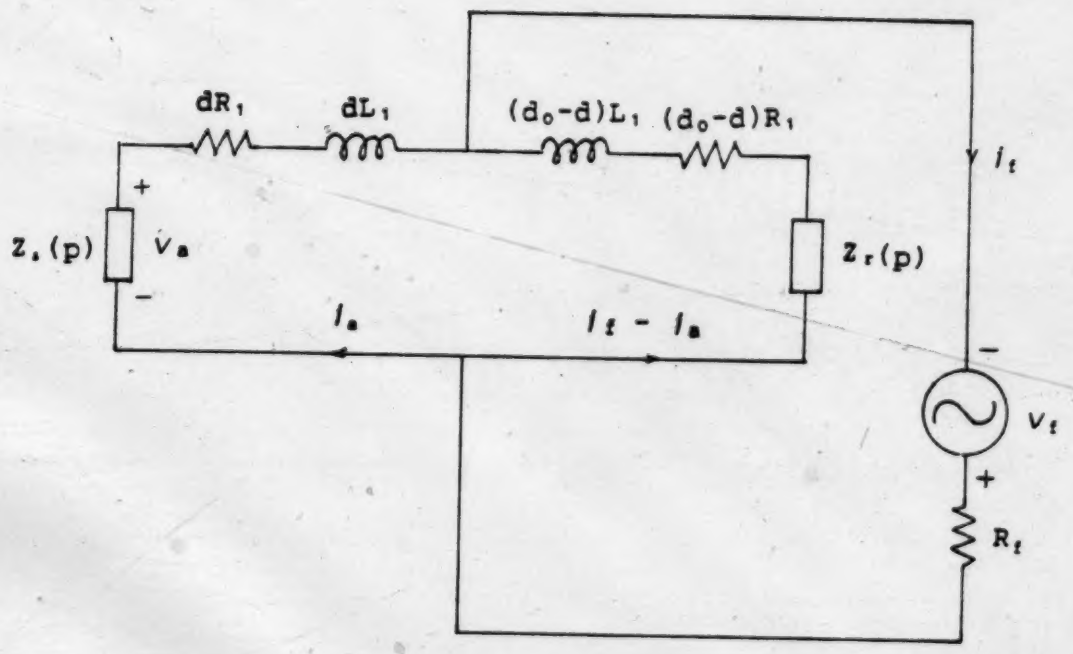

Figure 2.6 Network for a three phase fault

CHAPTER III

Fault Simulation (Real System)

3.1 Simulated Line with R-L Representation

A series R-L transmission line was formulated in order to test the fault locating algorithm. Oscillatory components will not be generated with the shunt capacitance excluded. Moreover, with this representation, the model developed in section 2.6 will be similar to the simplified simulated line (real system). Thus, the model output and the system output will have the same values if the same input is being used. Results for this system are included in Chapter Five. The general form of this lumped-parameter equivalent circuit is shown in Figure 3.1. Notice, the value of R and L in the Figure are the resistance and inductance per section respectively. Each section occupies a length of 12.5 miles, whereas the whole line is 100 miles long.

3.1.1 Simulation of Fault

Fault data can be determined from the state space model derived in the Appendix A2 together with the initial conditions (prefault data). The initial conditions required to start equation A2.3 are obtained from the steady state AC solution of the transmission line. The steady state solutions are then evaluated at the particular instant of application of the fault to yield the initial value of the

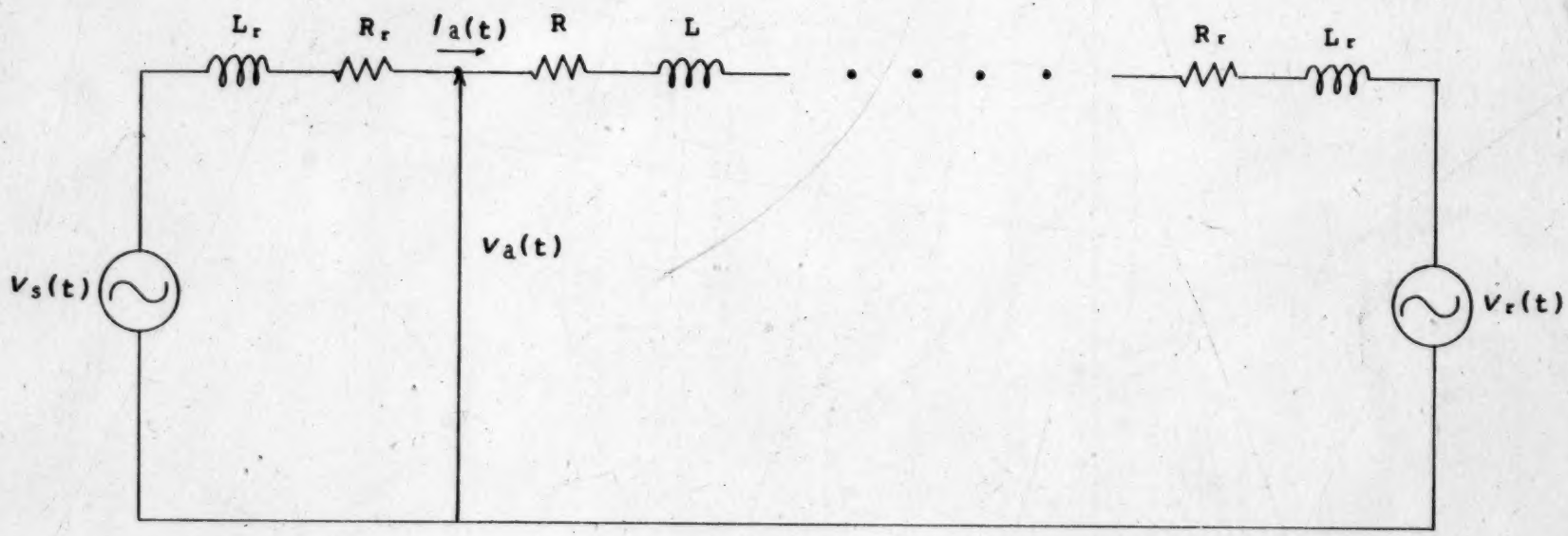

Figure 3.1 R-L series network

state X(0), which is required to solve equation A2.3. Its solution was solved by using Runge-Kutta numerical method and the results (postfault data) were stored and used as input data for the fault location algorithm. By varying N (number of sections) and the value of fault resistance, different sets of fault data can be obtained.

3.2 Simulated Line with π Section Representation

With the consideration of shunt capacitance, the dimension of the matrices or vectors in equation A2.3 will be increased. The inductor currents and the capacitor voltages are chosen as the state variables. It is well known that a uniform transmission line can be represented by a number of π sections connected in series. Therefore, eight π sections are arbitrarily chosen to represent a 100-mile transmission line. The general form of this lumped-parameter equivalent circuit is shown in Figure 3.2. Note that the values of R and L are resistance and inductance value per π section respectively.

3.2.1 Simulation of Fault

The state space representation of this system is also in the form of : $\dot{X} = A X + B U$. Instead of a 2x2 matrix, A is changed to a matrix of order 19x19. Also, X represents the state vector of order 19x1 ; B is a matrix of order 19x19 and U is the input vector of order 19x1. The state

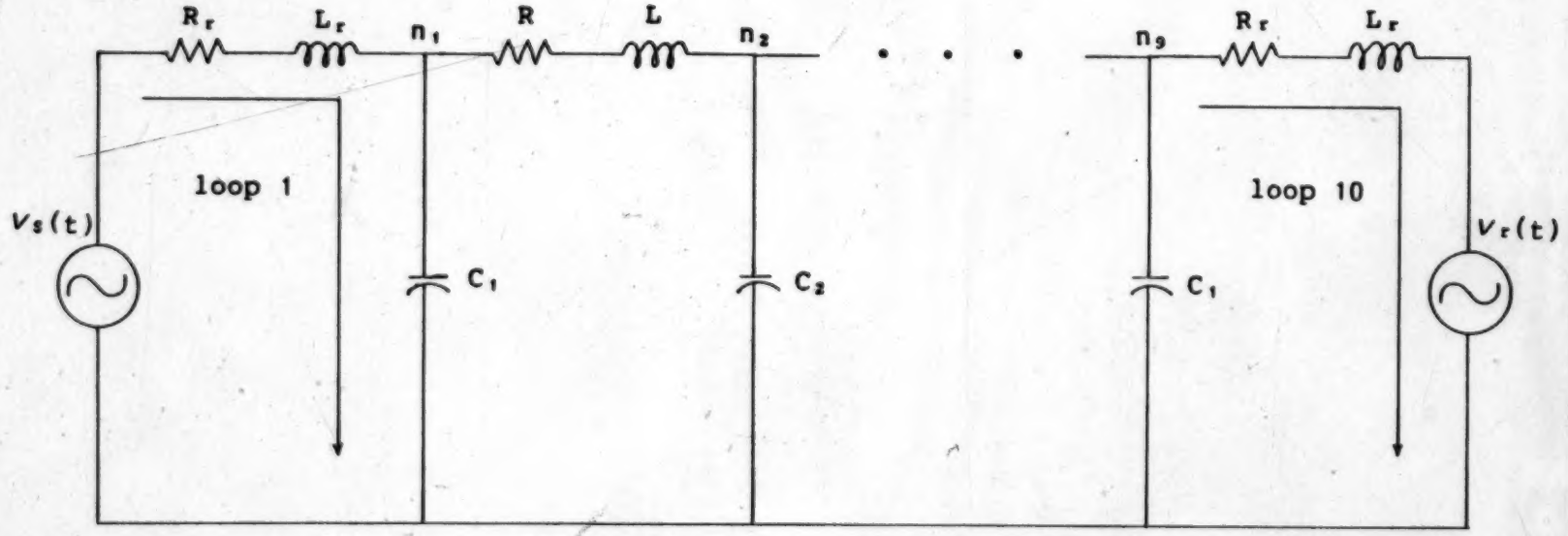

Figure 3.2 π section representation of transmission line

space model represented by a set of simultaneous first order differential equations is derived in Appendix A3. The prefault steady state solutions and the formulation of the state space equation are also included in this Appendix. To simulate a short circuit in the network, the required change is in the nodal equation of A3.2. For instance, a fault occurs at a distance of 25 miles, i.e. two π sections. The required change is in equation A3.2 of node number three. The new nodal equation becomes :

$$-I_3 + C_2\dot{V}_3 + I_4 + \frac{V_3}{R_f} = 0$$

or

$$\dot{V}_3 = \frac{I_3}{C_2} - \frac{I_4}{C_2} - \frac{V_3}{R_f * C_2} \qquad (3.1)$$

where, R_f is the fault resistance. Note that different fault distances can be simulated by changing the appropriate nodal equation.

3.3 Determination of Step Size for Numerical Solution of the Transmission Line

In order to determine the step size, eigenvalues of the characteristic matrix 'A' can be examined. For the eigenvalues of $-\gamma \pm j\omega$, its solution is in the form of $K_1 e^{-\gamma t}\cos(\omega t) + K_2 e^{-\gamma t}\sin(\omega t)$, where K_1 and K_2 are constants, determined by the initial conditions. Hence, the imaginary part indicates the frequency of oscillation of the

sinusoidal term, and the real part gives the time constant of the exponential decaying term. The cycle time of a sinusoid is $T=2\pi/\omega$, and the time constant of an exponential decaying term is $1/\gamma$. After these values are found, the step size is generally chosen to be the smaller value of T/100 or $(1/\gamma)/10$. Note that this criterion is flexible, and it has to be changed for different numerical methods because different methods provide different degrees of accuracy. With the inclusion of fault resistance, the matrix 'A' of equation A3.3 has to be changed. For instance, if a fault occurs at 25 miles, the required change is in the element of A(13,13). It has to be changed from zero to a value of $-1/(R_f*C_2)$. By using the circuit parameters given in Appendix A1 with the fault resistance of 0.12 p.u. (30Ω), the eigenvalues of 'A' were found with the help of IMSL mathematical library. Its values are tabulated in Table 3.1. From Table 3.1 the largest frequency of oscillation is $0.2054*10^{5}$ rad/second, which corresponds to T of $0.3059*10^{-3}$ seconds, and the largest exponential term is $-0.6037*10^{5}$/second, which corresponds to $1/\gamma$ of $0.1656*10^{-4}$ seconds. By looking at these values, a step size of $0.1*10^{-5}$ seconds is selected. Note that different fault resistances will yield different eigenvalues. Also, different fault distances will change the eigenvalues. Hence, step size has to be adjusted in each case.

Table 3.1 Eigenvalues of A with fault resistance of 0.12 p.u. (30Ω)

Real part	Imaginary part
-0.6037E+05	0.0
-0.1517E+02	0.2054E+05
-0.1517E+02	-0.2054E+05
-0.1434E+03	0.1928E+05
-0.1434E+03	-0.1928E+05
-0.3198E+02	0.1917E+05
-0.3198E+02	-0.1917E+05
-0.1133E+03	0.1647E+05
-0.1133E+03	-0.1647E+05
-0.1856E+03	0.1266E+05
-0.1856E+03	-0.1266E+05
-0.9247E+03	0.8347E+04
-0.9247E+03	-0.8347E+04
-0.3279E+02	0.8150E+04
-0.3279E+02	-0.8150E+04
-0.2552E+03	0.3139E+04
-0.2552E+03	-0.3139E+04
-0.1115E+02	0.0
-0.2157E+03	0.0

CHAPTER IV

Background of Least Squares Estimation Theory

4.1 Introduction

Least squares estimation method was first invented by Karl Gauss and was used practically for astronomical computations. Since that time the method of least squares has been applied for the solution of many technical problems. Although there are several other estimation methods available, such as maximum likelihood and minimum variance method, the least squares estimation is still one of the popular methods.

The block diagram of Figure 4.1 illustrates the basic idea of least squares algorithm. An input signal is fed into the real system when the model parameters are initialized with educated estimates. The error between the output from the real system and the model is used in the least squares algorithm to calculate the appropriate change in the parameters of the model so as to minimize the error. Then, this process is repeated with the parameters in the model updated in each iteration until no significant change in parameters is observed.

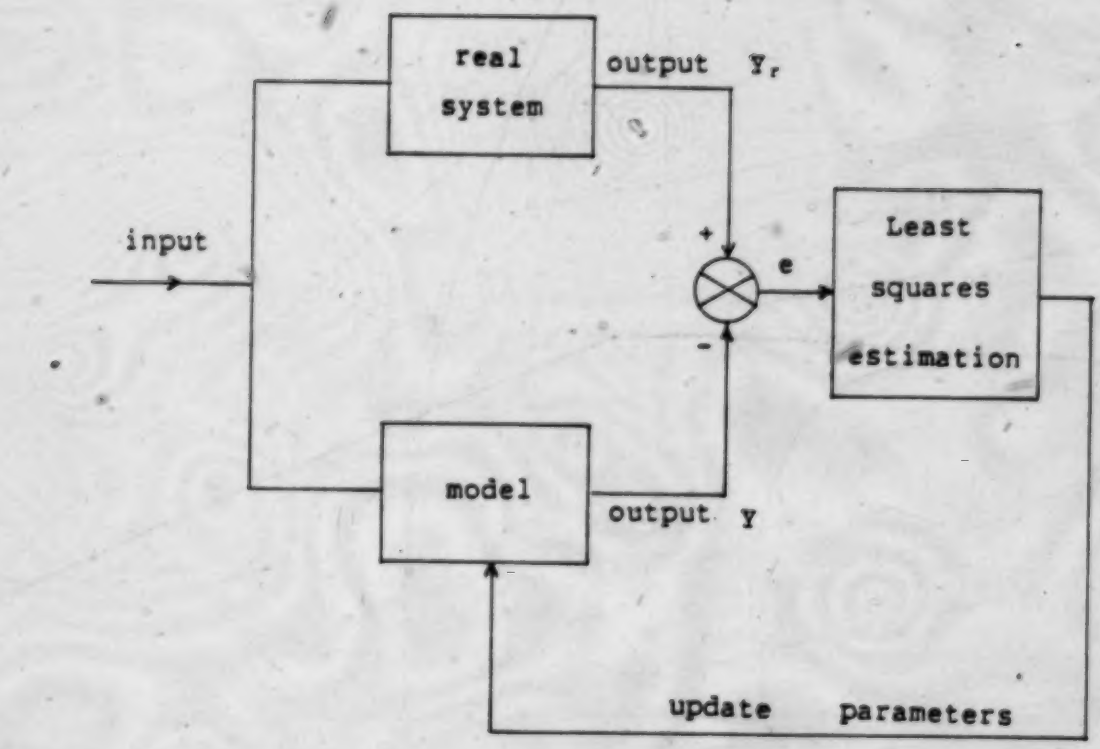

Figure 4.1 Least squares estimation system

4.2 Mathematical Formulation for the Least Squares Estimation Method

Let the model of Figure 4.1 be described by :

$$\dot{X} = A(\alpha)X + B(\alpha)U \tag{4.1}$$

$$X(t_o) = X_o \tag{4.2}$$

$$Y = C(\alpha)X \tag{4.3}$$

where,

X is the state vector of the model.
Y is the output vector from the model.
U is the input vector to the model and the real system.
$A(\alpha)$, $B(\alpha)$ and $C(\alpha)$ are coefficient matrices dependent on a parameter vector α, whose value is to be identified.

The cost function to be minimized can be formulated as :

$$J = \int_{t_o}^{t_k} (Y_r - Y)^T W (Y_r - Y) dt \tag{4.4}$$

where,

Y_r is the output vector from the real system excited with the same input as that of the model.

W is a positive definite weighting matrix.

T is the matrix transpose.

t_o is the initial observation time.

t_k is the final observation time.

Expanding the output Y in a Taylor series about its trajectory at a given value α_o of parameters α gives :

$$Y = Y(\alpha_o) + (\partial Y/\partial \alpha)_{\alpha_o}(\alpha-\alpha_o) + R \qquad (4.5)$$

where R is the higher order terms. α_o is the initial estimate of the parameter vector.

$\partial Y/\partial \alpha$ can be obtained from equation (4.3) as :

$$[\partial Y/\partial \alpha]_{\alpha_o} = C(\alpha_o)(\partial X/\partial \alpha)_{\alpha_o} + [\partial C(\alpha)/\partial \alpha]_{\alpha_o} X(\alpha_o) \qquad (4.6)$$

The time-dependent variables $(\partial X/\partial \alpha)_{\alpha_o}$ are found from the partial derivative of equation (4.1) relative to α and evaluated at α_o,

$$d[\partial X/\partial\alpha]_{\alpha_o}/dt = A(\alpha_o)(\partial X/\partial\alpha)_{\alpha_o} + [\partial A(\alpha)/\partial\alpha]_{\alpha_o} X(\alpha_o) \quad [\partial B(\alpha)/\partial\alpha]_{\alpha_o} U \tag{4.7}$$

$$[\partial X/\partial\alpha]_{\alpha_o, t_o} = 0 \tag{4.8}$$

By integrating equation (4.7), the variable $\partial X/\partial\alpha$ can be found, because

$$\partial X/\partial\alpha = \int_t^{t+\Delta t} \dot{(\partial X/\partial\alpha)}dt \tag{4.9}$$

Also the variable $X(\alpha_o)$ can be determined by integrating equation (4.1), evaluated at α_o, since

$$X = \int_t^{t+\Delta t} \dot{X}dt \tag{4.10}$$

Substitution of equation (4.5) in equation (4.4) yields,

$$J = \int_{t_o}^{t_k} [Y_r - Y(\alpha_o) - (\partial Y/\partial\alpha)_{\alpha_o}(\alpha-\alpha_o)]^T W \cdot [Y_r - Y(\alpha_o) - (\partial Y/\partial\alpha)_{\alpha_o}(\alpha-\alpha_o)]dt \tag{4.11}$$

Where the higher order terms of the expansion of Y are ignored.

Selecting the change in parameter $\Delta\alpha$ in order to minimize the cost function implies

$$\partial J/\partial(\alpha-\alpha_o) = 0 \tag{4.12}$$

where,

$$\Delta\alpha = \alpha-\alpha_o \tag{4.13}$$

from which follows a set of linear algebraic equations for $\Delta\alpha$:

$$\left[\int_{t_o}^{t_k} (\partial Y/\partial\alpha)^T_{\alpha_o} W(\partial Y/\partial\alpha)_{\alpha_o} dt\right]\Delta\alpha = \int_{t_o}^{t_k} [(\partial Y/\partial\alpha)^T_{\alpha_o} W(Y_r - Y(\alpha_o))]dt \tag{4.14}$$

After each period of integration, or observation, the appropriate change in parameter $\Delta\alpha$ can be found by solving the set of simultaneous algebraic equations generated by equation (4.14). Hence, estimate of α can be computed by the following formula :

$$\alpha^k = \alpha^{k-1}+G\Delta\alpha^k \tag{4.15}$$

where k =1,2,..... refers to the iteration count and α_0 is an initial estimate. In this study, G is selected as a constant matrix. Since the derivation assumes a sufficiently small $\Delta\alpha$, due to truncating the Taylor series, a gain matrix G has been inserted, whose elements are selected on the basis of computational judgment. G controls the extent of correction in each iteration step. The excessive large elements of G may cause α^k to overshoot and go into oscillation about $\hat{\alpha}$(true value), whereas the extremely small elements of G cause very slow convergence of α^k to $\hat{\alpha}$. A block diagram for the parameter estimation algorithm is shown in Figure 4.2.

4.3 Computational Aspect

Since the transmission line system and algorithm will be simulated in a digital computer, the discrete-time forms of some equations have to be used. Equation (4.4) has to be changed to

$$J = \sum_{i=1}^{K} [Y_r(i)-Y(i)]^T W(i)[Y_r(i)-Y(i)] \qquad (4.16)$$

where Y(i) and $Y_r(i)$, i=1,2,.....K, represent the sampled outputs of the model reference and real system respectively.

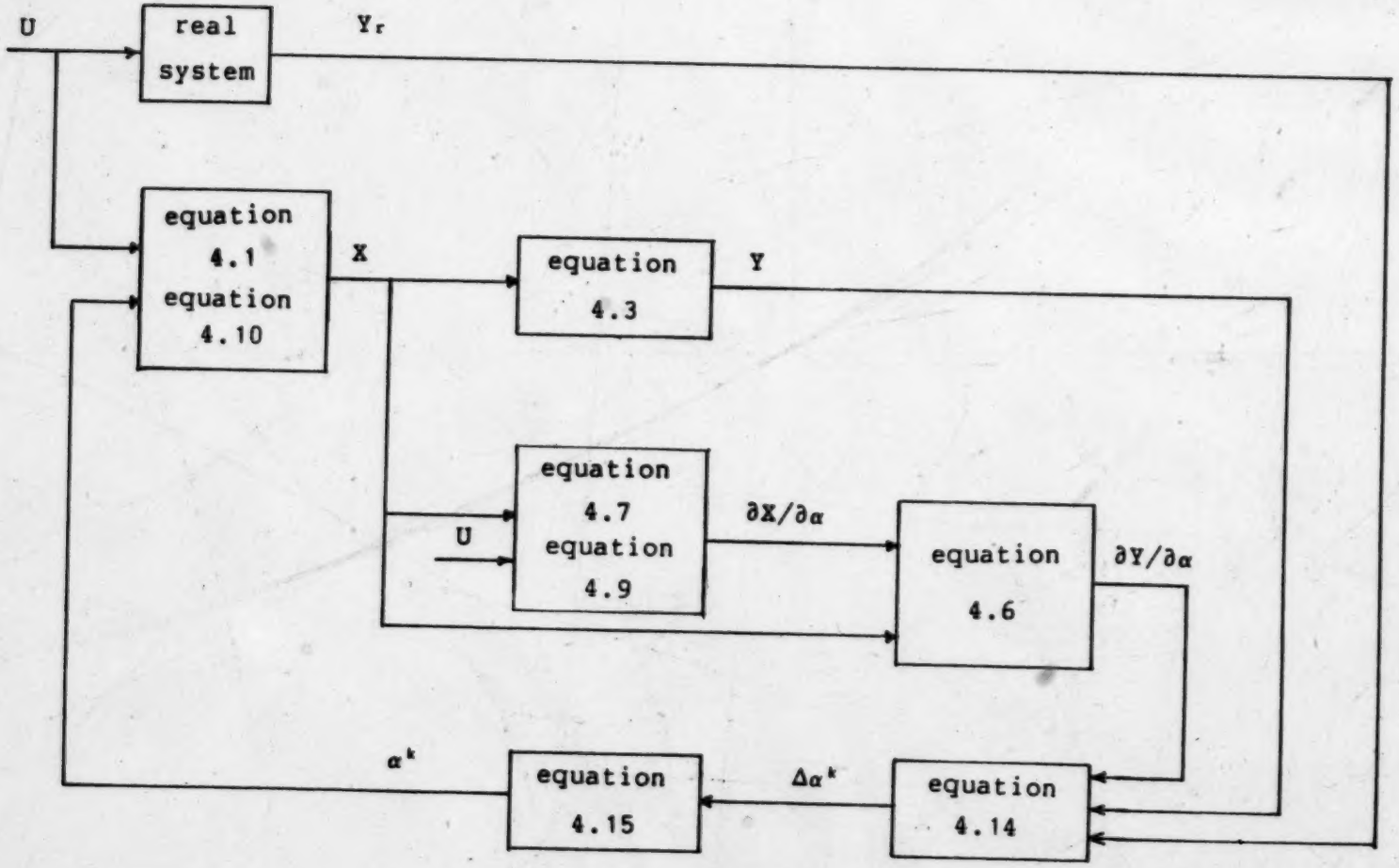

Figure 4.2 Algorithm of parameter estimation

Equation (4.11) is changed to

$$J = \sum_{i=1}^{K} \{Y_r(i)-Y(i,\alpha_o)-[\partial Y(i)/\partial\alpha]_{\alpha_o}(\alpha-\alpha_o)\}^T W(i)$$

$$\cdot\{Y_r(i)-Y(i,\alpha_o)-[\partial Y(i)/\partial\alpha]_{\alpha_o}(\alpha-\alpha_o)\} \qquad (4.17)$$

Also, equation (4.14) becomes

$$\{\sum_{i=1}^{K} [\partial Y(i)/\partial\alpha]_{\alpha_o}^T W(i)[\partial Y(i)/\partial\alpha]_{\alpha_o}\}(\Delta\alpha)$$

$$= \sum_{i=1}^{K} [\partial Y(i)/\partial\alpha]_{\alpha_o}^T W(i)[Y_r(i)-Y(i,\alpha_o)] \qquad (4.18)$$

Let the number of outputs be m, and the number of parameters be n. Assume W(i) as a square matrix with dimension of mxm. In equation (4.18), the dimension of $[\partial Y(i)/\partial\alpha]$ is mxn, $\Delta\alpha$ is a nx1 vector, and $[Y_r(i)-Y(i,\alpha_o)]$ is a mx1 vector. Hence, equation (4.18) represents n simultaneous algebraic equations. In order to solve for $\Delta\alpha$ from equation (4.18), the equation can be written as :

$$\Delta\alpha = \{\sum_{i=1}^{K} [\partial Y(i)/\partial\alpha]_{\alpha_o}^T W(i)[\partial Y(i)/\partial\alpha]_{\alpha_o}\}^{-1}$$

$$\{\sum_{i=1}^{K} [\partial Y(i)/\partial\alpha]_{\alpha_o}^T W(i)[Y_r(i)-Y(i,\alpha_o)] \qquad (4.19)$$

The difficulty in solving $\Delta\alpha$ by equation (4.19) is to compute the inversion of a matrix of dimension nxn. The more parameters there are, the larger n becomes, and more computing time is requried to calculate the inverse. One way to overcome the above difficulty is to solve for $\Delta\alpha$ directly from the normal equation (4.18), using technique such as Gauss's elimination. If value of n is large and minimum computing time is one of the key concerns, solving for $\Delta\alpha$ with equation (4.18) is preferred.

Recursive identification algorithm requires continuous fault data input while the parameter is being estimated. The method could not be used in the fault location algorithm since the fault data are only available up to the instant the line is tripped. This constraint dedicated that the batch algorithm used in this project was one of the applicable techniques.

CHAPTER V

Least Squares Estimator

5.1 Application to Fault Location for a Single Line to Ground Fault

A single line to ground fault on phase 'a' is considered as a first test for applying least squares parameter estimation. In the following, the network equations of the model (equation 2.5) are written in state space form as required by equation (4.1), with the currents i_k, k = 0,1,f, selected as the system state variables. The voltages v_k, k = 0,1,f, are selected as the known input variables, and the unknown parameters d and R_f are chosen as the parameter vector α, whose values are to be estimated. Note that v_f is determined from equation (2.6) and (2.7) together with $\bar{V}_a$ and $\bar{I}_a$, and it is also updated each time with new estimated parameter vector. The currents i_0 and i_1 are selected as the model outputs which are compared with the values obtained from the actual line fault-caused currents to find the unknown parameters d and R_f. Thus the state vector is

$$X = \begin{bmatrix} i_0 \\ i_1 \\ i_f \end{bmatrix} \qquad (5.1)$$

The known input vector U is

$$U = \begin{bmatrix} v_o \\ v_1 \\ v_f \end{bmatrix} \tag{5.2}$$

and the output vector Y is

$$Y = \begin{bmatrix} i_o \\ i_1 \end{bmatrix} \tag{5.3}$$

Rearranging equation (2.5) yields

$$\dot{i}_o = \{-(d_oR_o+R_{ro})i_o + [(d_o-d)R_o+R_{ro}]i_f + [(d_o-d)L_o+L_{ro}]\dot{i}_f+v_o\}/(d_oL_o+L_{ro}) \tag{5.4}$$

$$\dot{i}_1 = \{-(2d_oR_1+2R_{r1})i_1+[2(d_o-d)R_1+2R_{r1}]i_f + [2(d_o-d)L_1+2L_{r1}]\dot{i}_f+2v_1\}/(2d_oL_1+2L_{r1}) \tag{5.5}$$

$$\dot{i}_f = \{[(d_o-d)R_o+R_{ro}]\dot{i}_o+[2(d_o-d)R_1+2R_{r1}]\dot{i}_1$$

$$-[(d_o-d)(R_o+2R_1)+R_{ro}+2R_{r1}+3R_f]i_f$$

$$+[(d_o-d)L_o+L_{ro}]\dot{i}_o + [2(d_o-d)L_1+2L_{r1}]\dot{i}_1$$

$$+\sqrt{3}v_f\}/[(d_o-d)(L_o+2L_1)+L_{ro}+2L_{r1}] \qquad (5.6)$$

Note that in equation (5.6), $\dot{i}_f$ also depends on the derivatives of state variable i_o and i_1. Hence, the substitution of $\dot{i}_o$ in equation (5.4) and $\dot{i}_1$ in equation (5.5) into equation (5.6) is made before any computation. After the substitution, $\dot{i}_f$ can be written as :

$$\dot{i}_f = f(X,U,\alpha) \qquad (5.7)$$

The complete expression of equation (5.7) can be found in Appendix A4. Instead of expressing equations (5.4), (5.5) and (5.7) in the form of state space equation (4.1), they are kept in the original form. In order to compute the derivative of the state vector X, the equations have to be evaluated in the sequence order of equation (5.7), equation (5.4) and equation (5.5).

Since the model of Figure 2.5 is formulated with fault-caused component, prefault data have to be subtracted

from the postfault data before the algorithm. The prefault voltage $\bar{V}_a$ and current $\bar{I}_a$ at the measurement point, whose values can be found by following the method in Appendix A3.1, are also required by the algorithm.

A block diagram for the estimation algorithm is shown in Figure 5.1. The inputs v_0 and v_1 are the real parts of the symmetrical components of the fault-caused part of the observed voltages v_{abc}. The prefault voltage and current, $\bar{V}_a$ and $\bar{I}_a$ are complex constants. Each iteration step consists of generating model output of $i_{0,f}$ and partial derivatives at each sample point using equations (5.7), (5.4), (5.5) and equation (4.7) respectively, advancing to the next sample point and accumulating the partial derivatives and errors in accordance with equation (4.18) until the end of sampling interval. Then the parameter vector is updated with equation (4.15).

5.2 Application to Fault Location for a Three Phase Fault

For this balanced fault, the structure of the estimator is simpler. The network equations of the model, equations (2.8) and (2.9) are written in state space form as required by equation (4.1), with the current i_k, k =a,f, selected as the system state variables. The voltages v_k, k =a,f, are selected as the known input variables and the unknown parameter vector α whose value is to be estimated. The current i_a is selected as the model output, which is

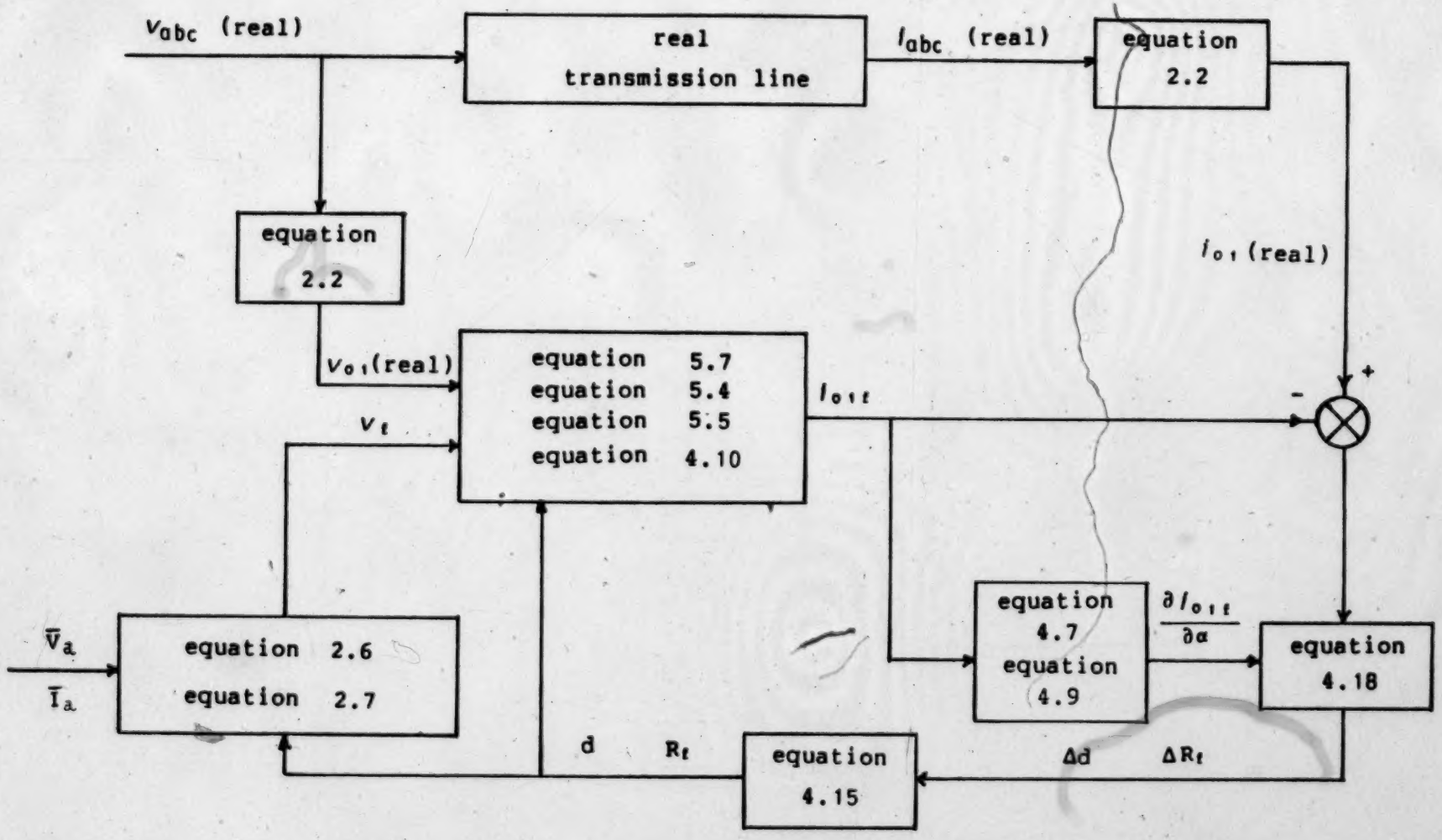

Figure 5.1 Algorithm of parameter estimation for single line to ground fault

compared with the value obtained from the actual line fault-caused current to find the unknown parameters d and R_f. Hence, the state vector X is

$$X = \begin{bmatrix} i_a \\ i_f \end{bmatrix} \tag{5.8}$$

the known input vector U is,

$$U = \begin{bmatrix} v_a \\ v_f \end{bmatrix} \tag{5.9}$$

and the output Y is a scalar of i_a,

$$Y = i_a \tag{5.10}$$

By rearranging equations (2.8) and (2.9), the model equations become :

$$\dot{i}_a = \{-(d_o R_1 + R_{f1})\, i_a + [(d_o - d)R_1 + R_{f1}]\, i_f + [(d_o - d)L_1 + L_{f1}]\, \dot{i}_f + v_a\} / (d_o L_1 + L_{f1}) \tag{5.11}$$

$$\dot{i}_f = \{[(d_o-d)R_1+R_{r1}]\dot{i}_a - [(d_o-d)R_1+R_{r1}+R_f]i_f$$

$$+[(d_o-d)L_1+L_{r1}]\dot{i}_a + v_f\}/[(d_o-d)L_1+L_{r1}] \quad (5.12)$$

Again, in equation (5.11), $\dot{i}_a$ depends on the derivatives of state variable i_f. Hence, the substitution of equation (5.11) into equation (5.12) is necessary. Thus $\dot{i}_f$ can be written as :

$$\dot{i}_f = f(X,U,\alpha) \quad (5.13)$$

The expression of equation (5.13) can be found in Appendix A5. A lot of algebra is involved in expressing equations (5.11) and (5.12) in the form of equation (4.1). They are kept in the original form for the sake of simplicity. In order to compute the derivative of state vector X, the equations have to be evaluated in the order of equation (5.13) and equation (5.11). Since the model of Figure 2.6 is formulated in fault-caused component, prefault data have to be subtracted from the postfault data before the algorithm. The known prefault voltage $\bar{V}_a$ and $\bar{I}_a$ at the measurement point, derived in Appendix A2.1, have to be inserted into the algorithm. A block diagram for this algorithm is shown in Figure 5.2.

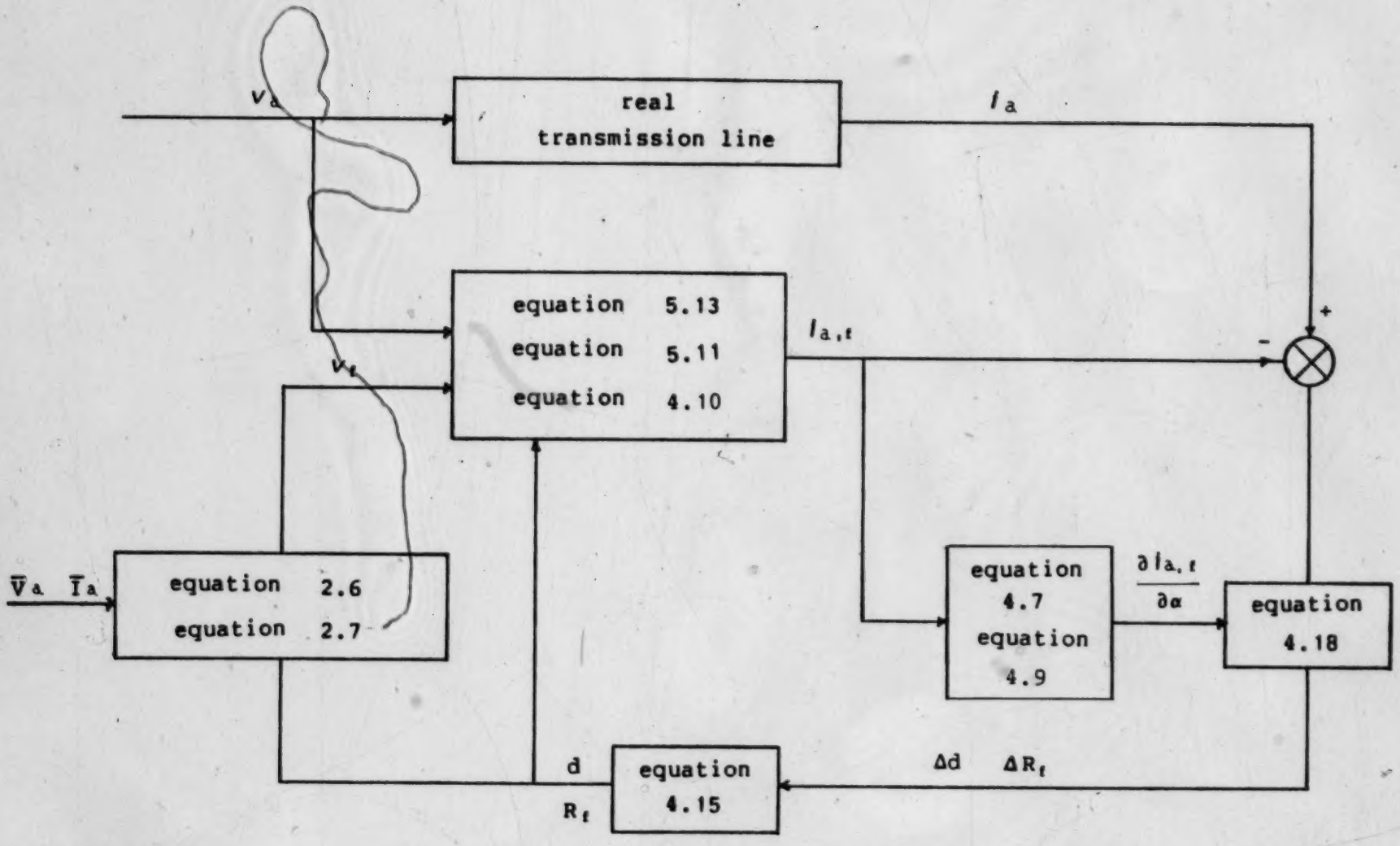

Figure 5.2 Algorithm of parameter estimation for three-phase fault

5.3 Discussion of Results

In order to test the algorithm, three different kinds of tests are set up. The descriptions of systems and models in different tests are summarized in Table 5.1. Tests one and two are used to study three phase fault. Test three is used to study a single line to ground fault. By the principle of superposition, postfault data consist of prefault data and fault-caused data. Since the models were formulated to use the fault-caused component, prefault data in the system have to be subtracted from the postfault data in the system before the algorithm is applied.

For all tests, the initial estimates are chosen as d=0.5 and R_f=0.01, and the weighting matrices are equal to unity. From Figure 5.9 to Figure 5.12, for all tests with a given data window, the number of iterations required to converge to the final estimated value is in the range of 20 to 40. By the well known sampling theorem, the aliasing effect will be reduced by using a sampling frequency of at least twice the highest frequency of the observed transient components. Hence, a sampling period of $1*10^{-5}$ seconds is used with Euler's integration method in the estimator.

Typical transient voltages and currents of one power cycle (60Hz) are shown in Figure 5.3 to Figure 5.6. Figure 5.3 and Figure 5.4 are the transient response of the simulated R-L series transmission line. Figure 5.5 and Figure 5.6 show the transient response of a transmission

Table 5.1 Descriptions of Systems and Models Used in Different Tests

	Real System	Model
Test 1	single phase, R-L series representation of transmission line.	single phase, R-L series representation of transmission line.
Test 2	single phase, π section representation of transmission line.	single phase, R-L series representation of transmission line.
Test 3	single phase, π section representation of transmission line. Using symmetrical transformation to provide positive, negative and zero sequence quantities, with the assumption that mutual coupling between phases are neglected.	symmetrical sequence impedance network, R-L series representation of transmission line.

line represented by eight π sections. These figures show that the R-L representation gives a smooth response, whereas the π section representation introduces oscillatory effect. Note that the time axis is scaled from the instant of fault application. In other words, only postfault data are shown.

5.3.1 Effect of G on Estimator Convergence

As mentioned in section 4.2, G controls the extent of correction in each iteration step. A large value of G may cause the estimator to diverge. Too small a value will give slow convergence. For this study, only test one was used to illustrate the effect of G. In this test, G was chosen as a diagonal matrix with element g_{ii}. In Figure 5.7, $g_{ii}=2$ for $i=1,2$ and with this gain the estimated value oscillates around the true value. In Figure 5.8, $g_{ii}=0.4$ for $i=1,2$, which makes the estimator converge to the true value with approximately twenty iterations. By comparing Figure 5.7 and Figure 5.8, it is noted that a gain of 2 is too large for this algorithm, whereas, a gain of 0.4 is a better choice. Note that the extent of oscillation and the convergence depend on the value of the gain and on the algorithm.

5.3.2 Effect of Changing Fault Distance on Location Accuracy

Figure 5.9 to Figure 5.11 show the effects of changing the fault distance on location accuracy for different tests. From Figure 5.9 to Figure 5.11, the actual fault distance

was changed from 25 miles to 75 miles, in steps of 25 miles. Test one shows the fastest convergence to the true value within a data window of four milliseconds. For this test, the convergence to the true value for a one millisecond data window was also recorded. Test two shows the consistent shape of convergence. For a data window of twenty milliseconds, the relative error between the estimated value and the true value is found in the range of 6 to 12 %. Note that a larger data window yields a more accurate estimate. Test three also shows a consistent shape of convergence, but a bias problem exists. This is not caused from the measurement data, since all the input data are noise free. It may be due to the fact that the simulated eight π section transmission line (real system) ignored the mutual coupling between phases, but the derived model in section 2.4 suggests the coupling implicity. This aspect will be illustrated in Appendix A6. Generally, the changing of fault distance will not affect the accuracy and the convergence.

5.3.3 Effect of Changing Fault Resistance on Location Accuracy

Figure 5.10 and Figure 5.12 demonstrate the insensitivity of the algorithm to the change of fault resistance. Fault resistance is changed from 0.12 p.u. (30Ω) to 0.004 p.u. (1Ω), and fault distance is kept the same (50 miles). Test one does not seem to have any response to the change. For tests two and three, they both start at

different estimated values at four milliseconds, but they eventually approach the true value. Again, due to the previously discussed error source, test three also has a bias problem. Despite this discrepancy, the change of fault resistance will not affect the location accuracy.

5.3.4 Reconstruction of Waveform

Using initially assumed parameters and the identified parameters, different model outputs can be reproduced. They are then compared with their corresponding system outputs to show the resemblance between them. These results are shown from Figure 5.13 to Figure 5.20.

With initial estimates chosen near zero, all models outputs are significantly different from their corresponding system outputs. Then, the models will adjust themselves in order to minimize the cost function of equation 4.16. In Figure 5.13, Figure 5.15, Figure 5.17, and Figure 5.19, the extent of discrepancy between models and systems are shown. Note that, due to the large magnitudes of the initial model outputs, the corresponding system outputs are relatively straight when plotted on the same graphs. Figure 5.14, Figure 5.16, Figure 5.18, and Figure 5.20 demonstrate the effect of least squares estimator. As a result, the error between the model and the system is reduced drastically.

5.3.5 Modelling Error

The model and system used in test one are exact duplicates of each other. In test number two, the insertion of shunt capacitance in the π section representation introduces a discrepancy between the system and the model. Hence, the structure of the model is only an approximation to the real system. Using a symmetrical transformation, and neglecting the effect of mutual coupling for the system in test number three, the structural difference between the system and the model is even more pronounced. Hence, except in test number one, the model output and system output generated in test number two and those generated in test number three, are not expected to be the same due to modelling approximation.

The results shown in Figure 5.14, Figure 5.16, Figure 5.18 and Figure 5.20 prove this point. In order to model a transmission line exactly, a distributed parameter model is preferred. However, using this model is not a practical measure, for it will result in a heavy computational burden. Therefore, a much longer time will be expected for the estimator to locate a fault.

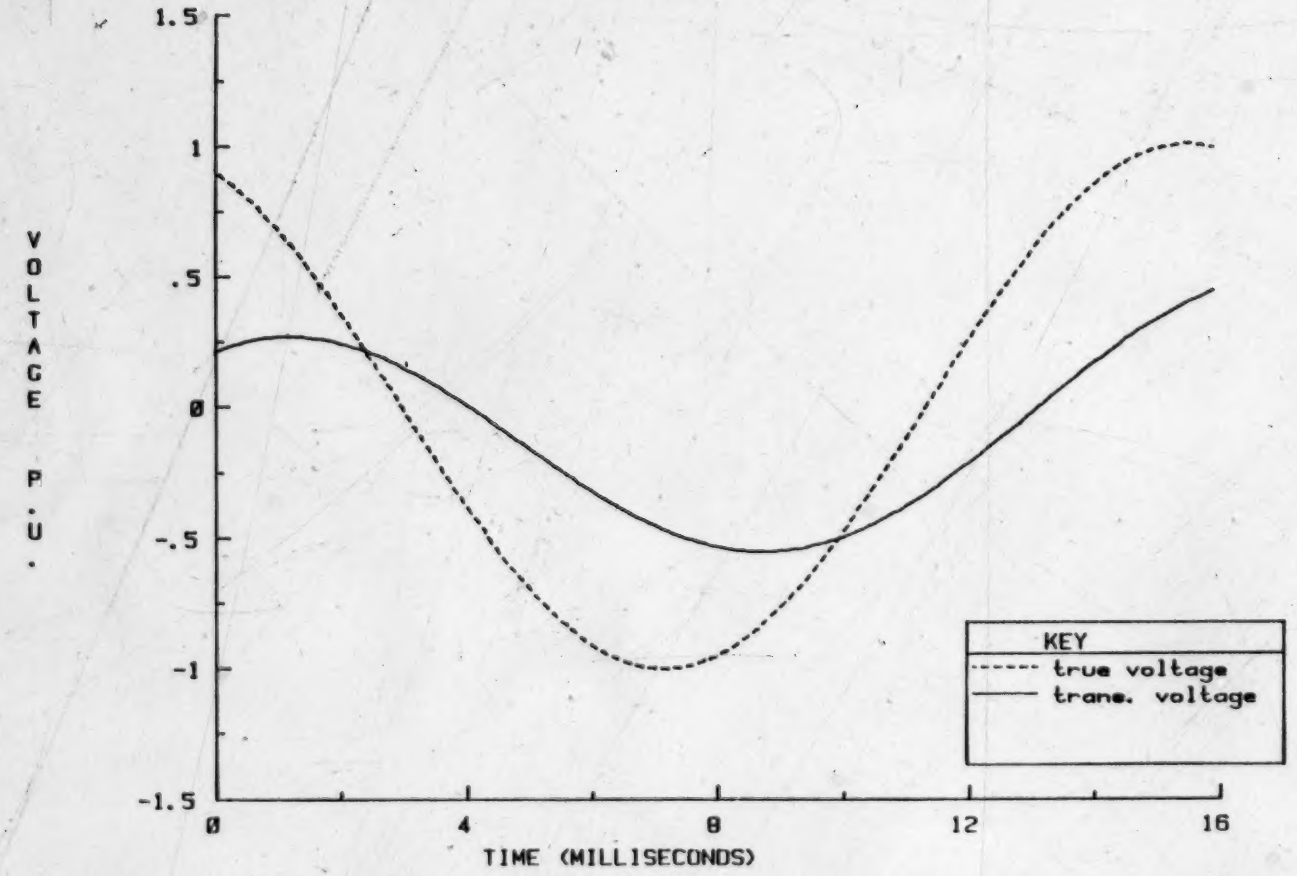

Figure 5.3 Typical transient voltage of R-L transmission line

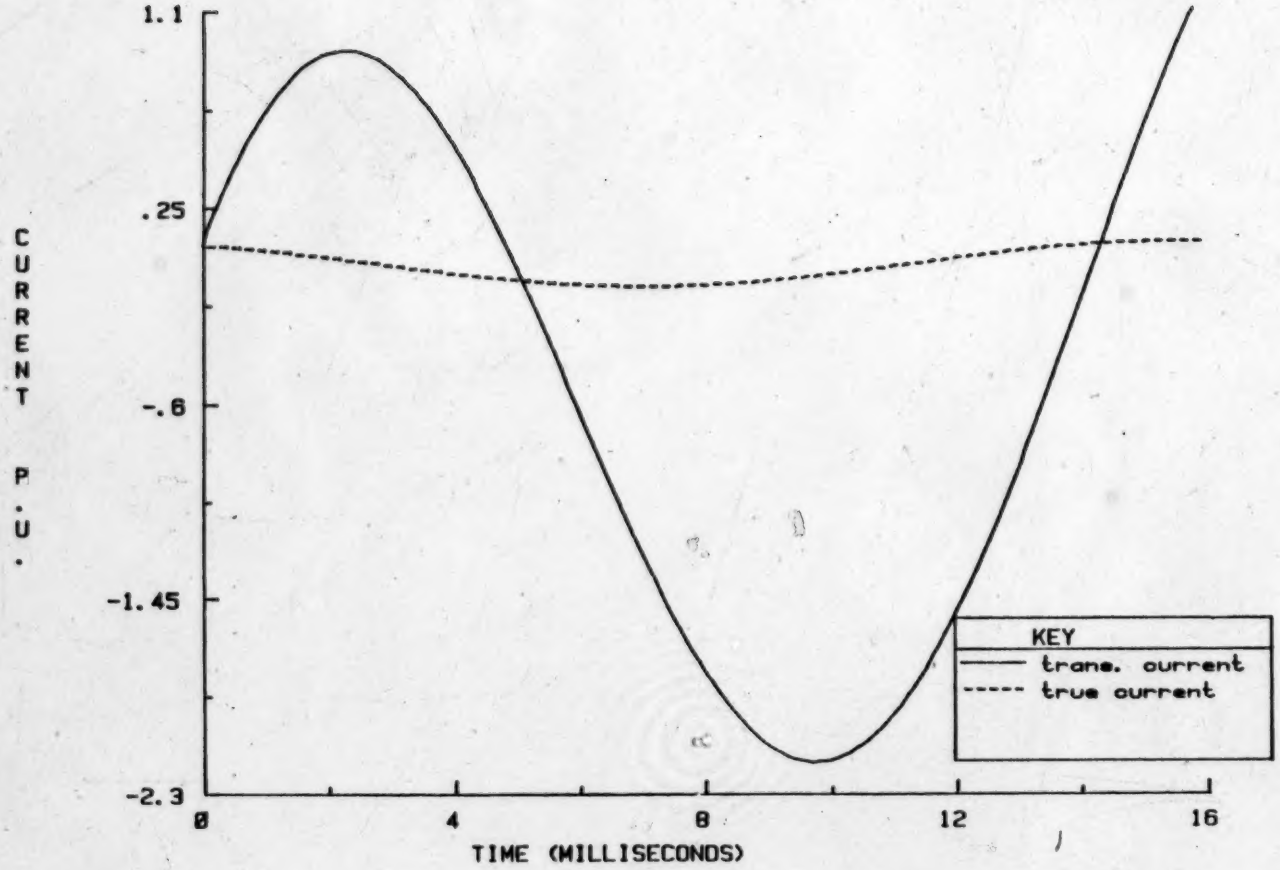

Figure 5.4 Typical transient current of R-L transmission line

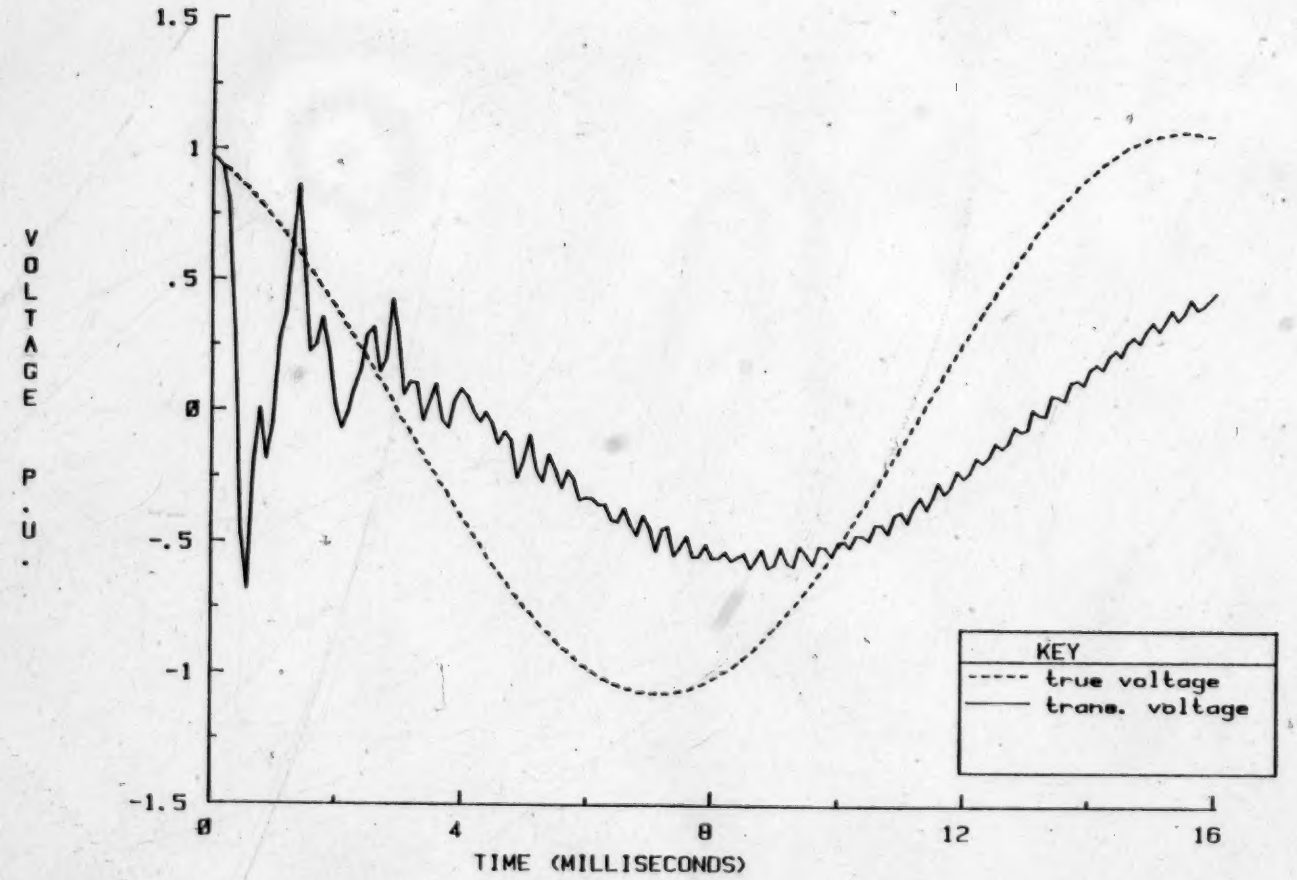

Figure 5.5 Typical transient voltage of π section transmission line

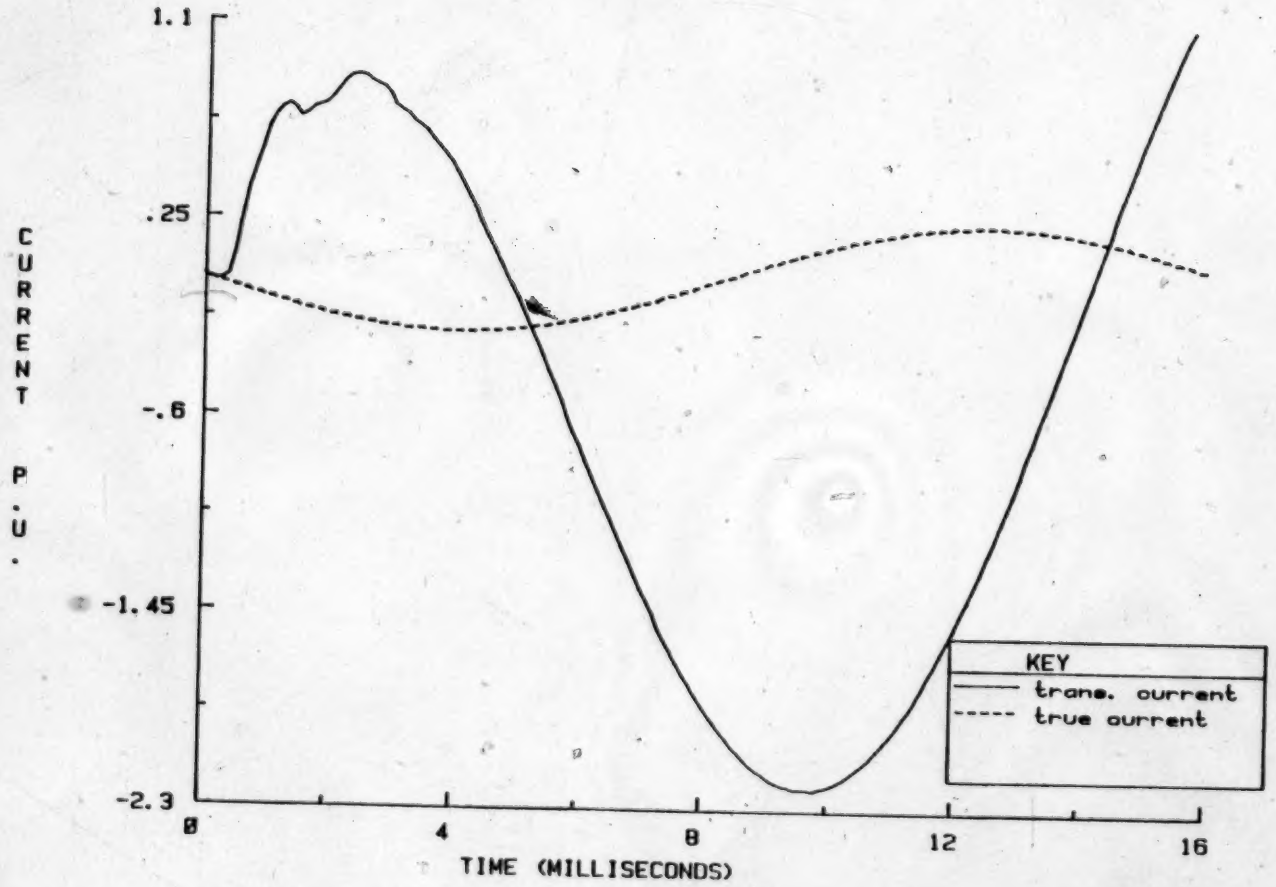

Figure 5.6 Typical transient current of π section transmission line

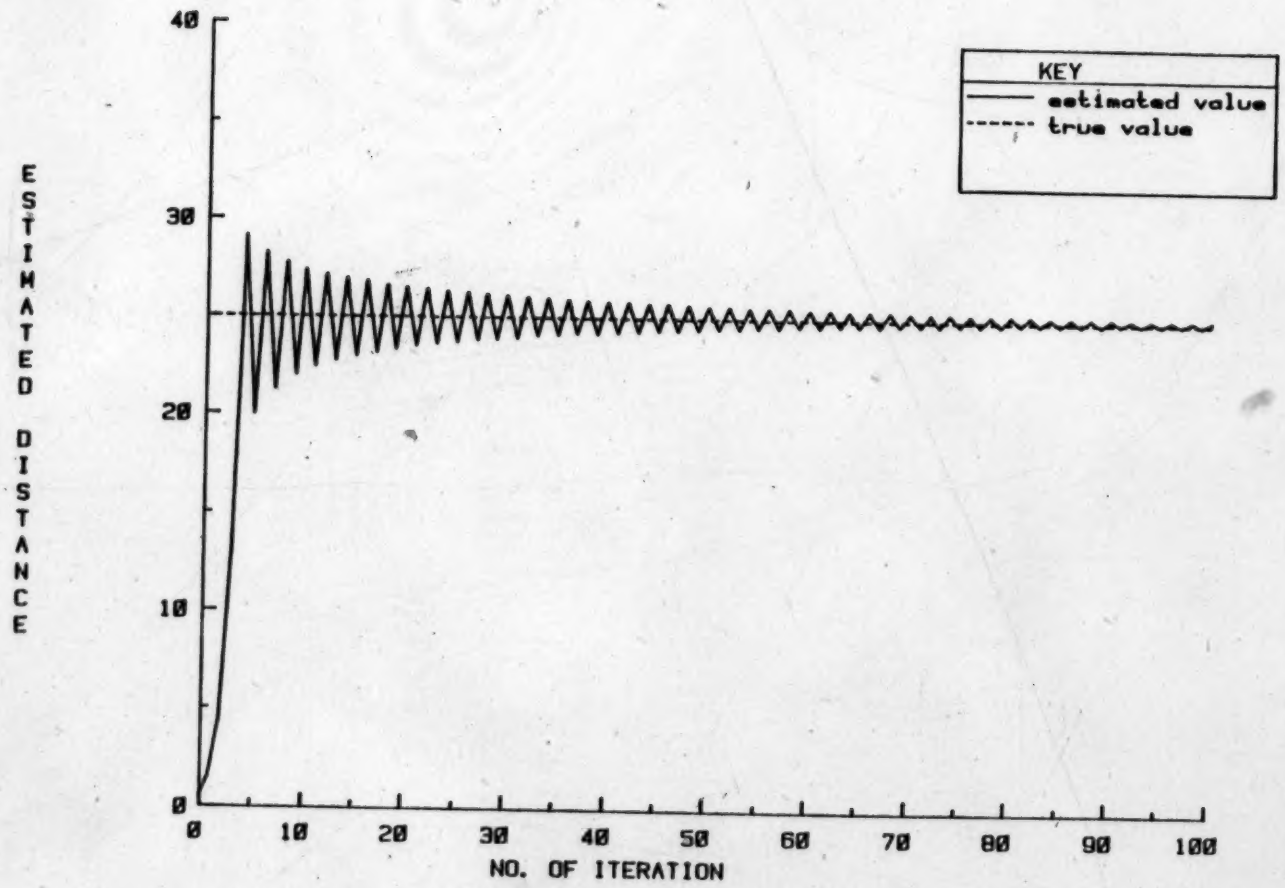

Figure 5.7 Effect of G on algorithm, with g_{α} = 2.0

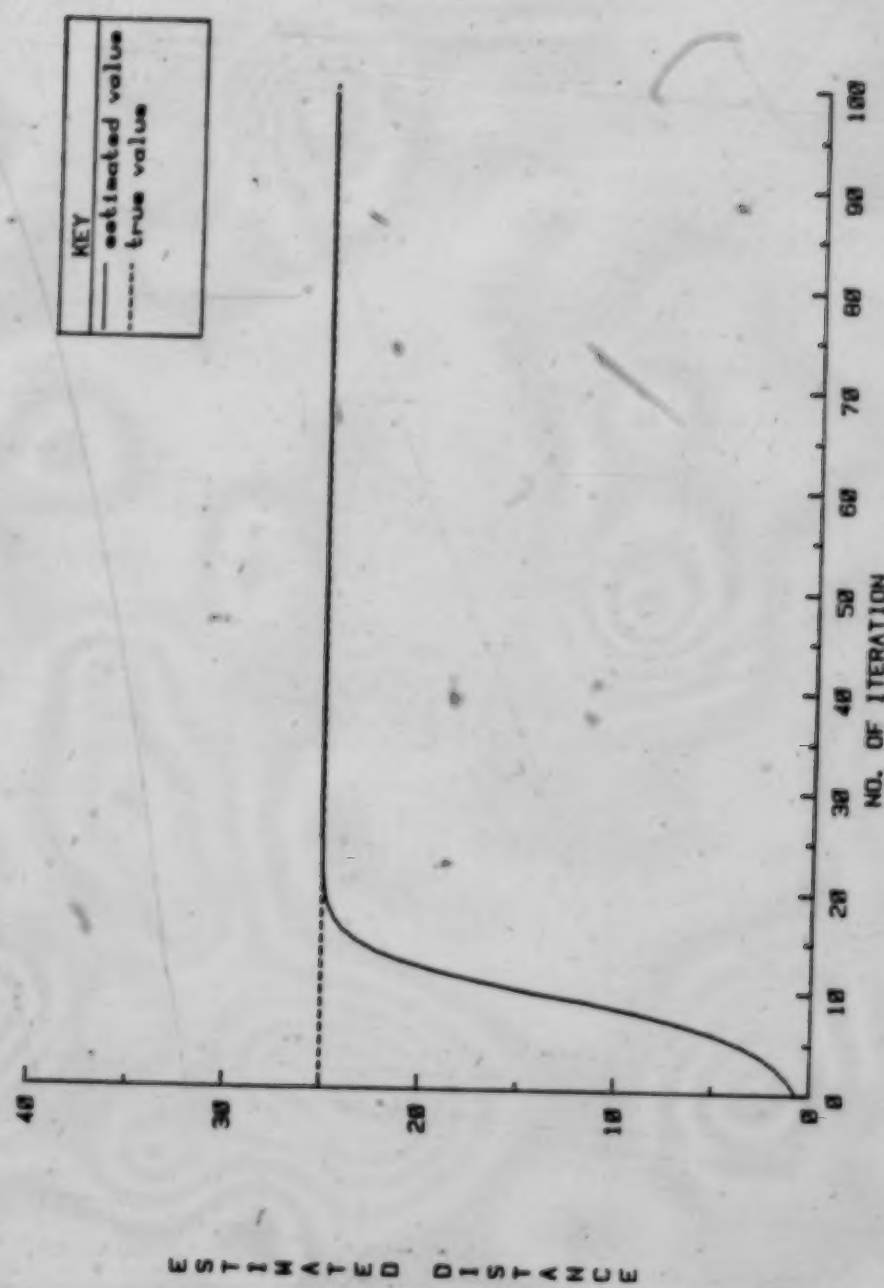

Figure 5.8 Effect of G on algorithm, with g_{11}= 0.4

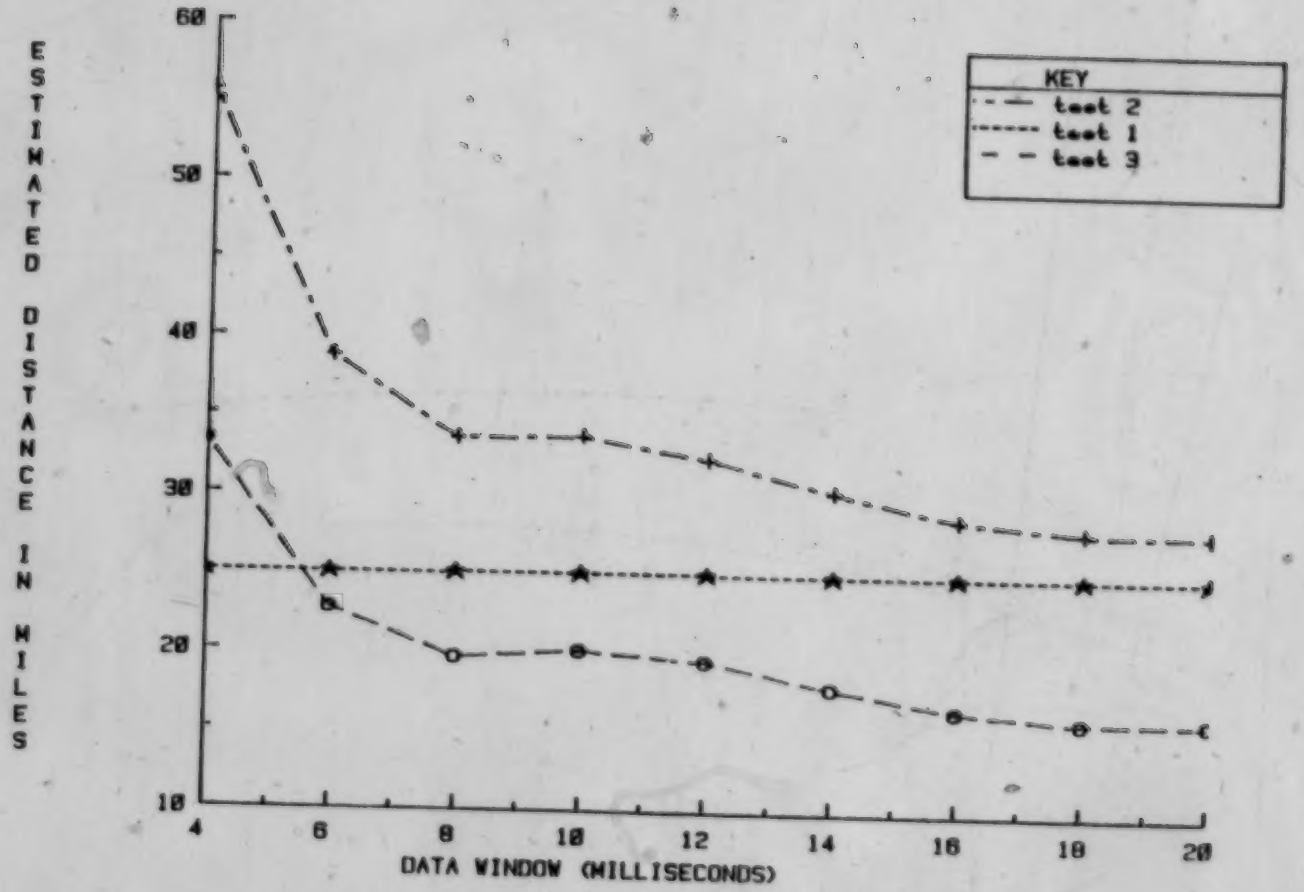

Figure 5.9 Estimated distance versus data window with actual fault distance of 25 miles and fault resistance of 0.12 p.u.

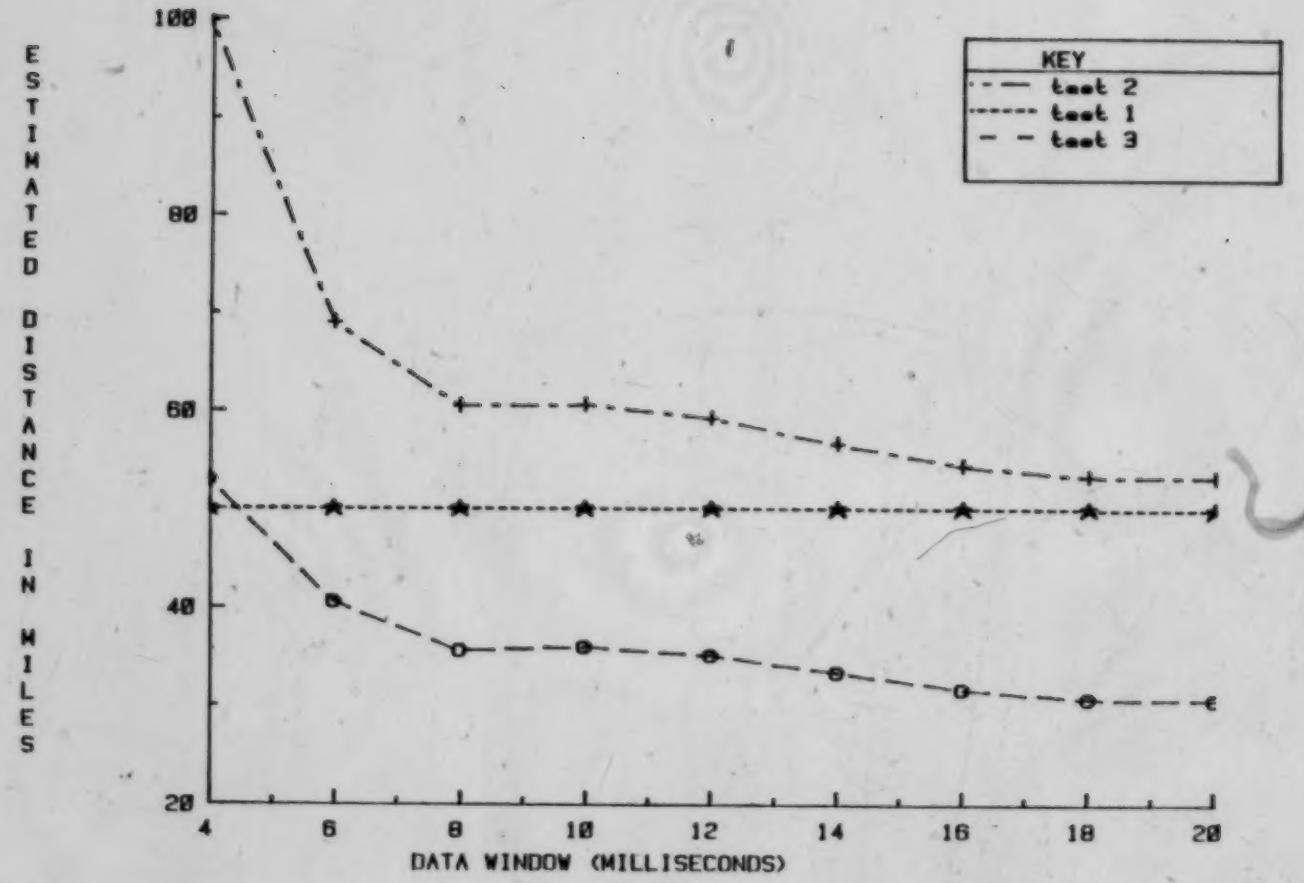

Figure 5.10 Estimated distance versus data window with actual fault distance of 50 miles and fault resistance of 0.12 p.u.

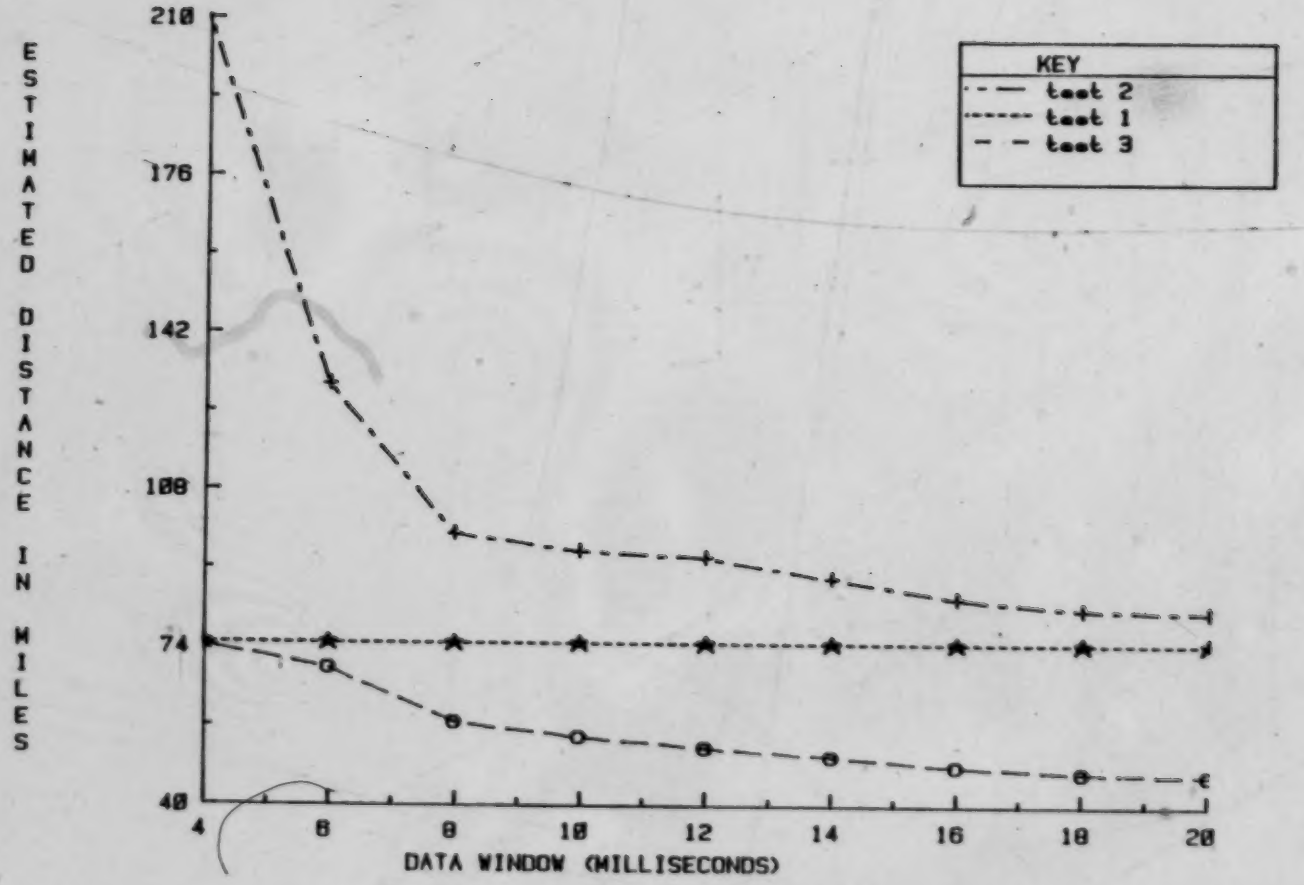

Figure 5.11 Estimated distance versus data window with actual fault distance of 75 miles and fault resistance of 0.12 p.u.

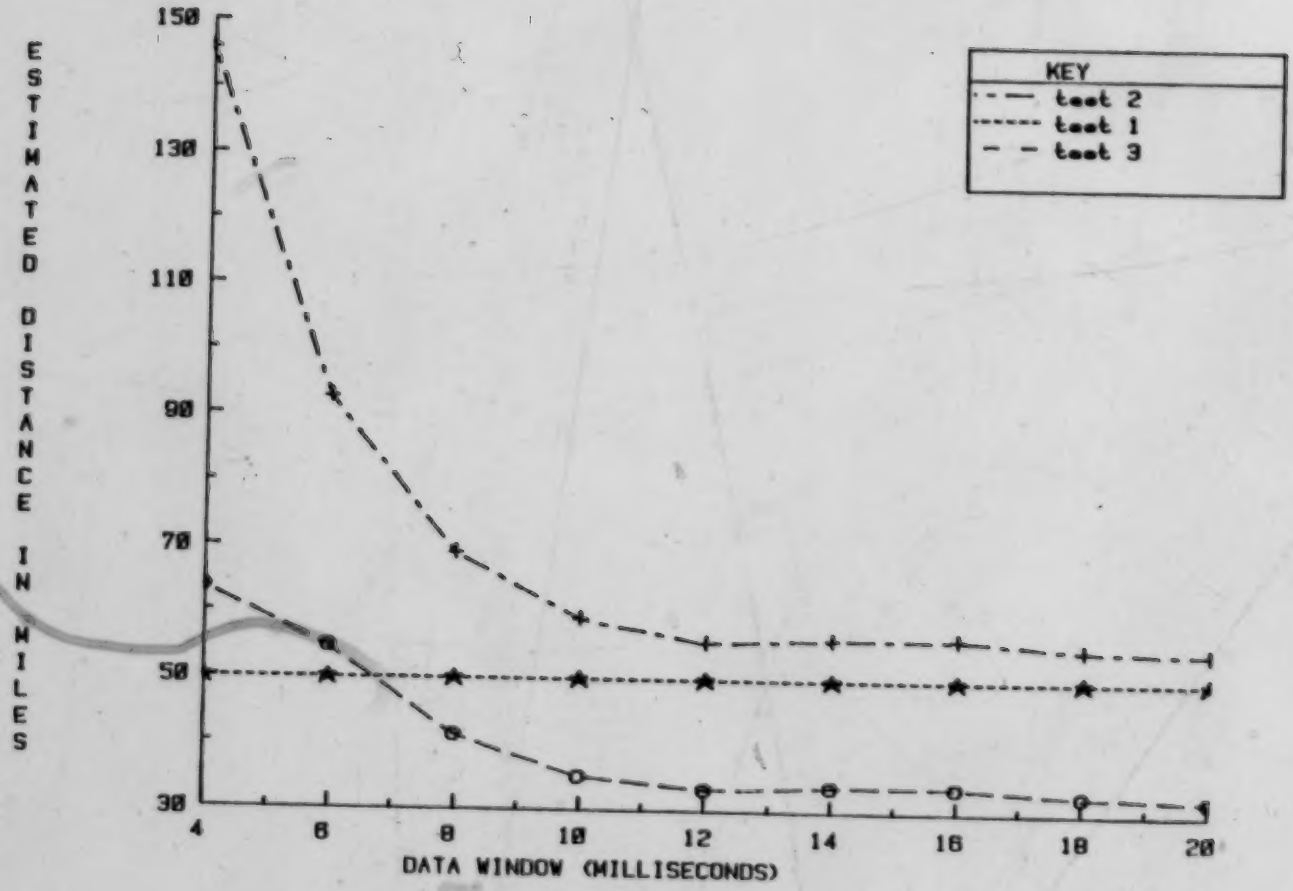

Figure 5.12 Estimated distance versus data window with actual fault distance of 50 miles and fault resistance of 0.004 p.u.

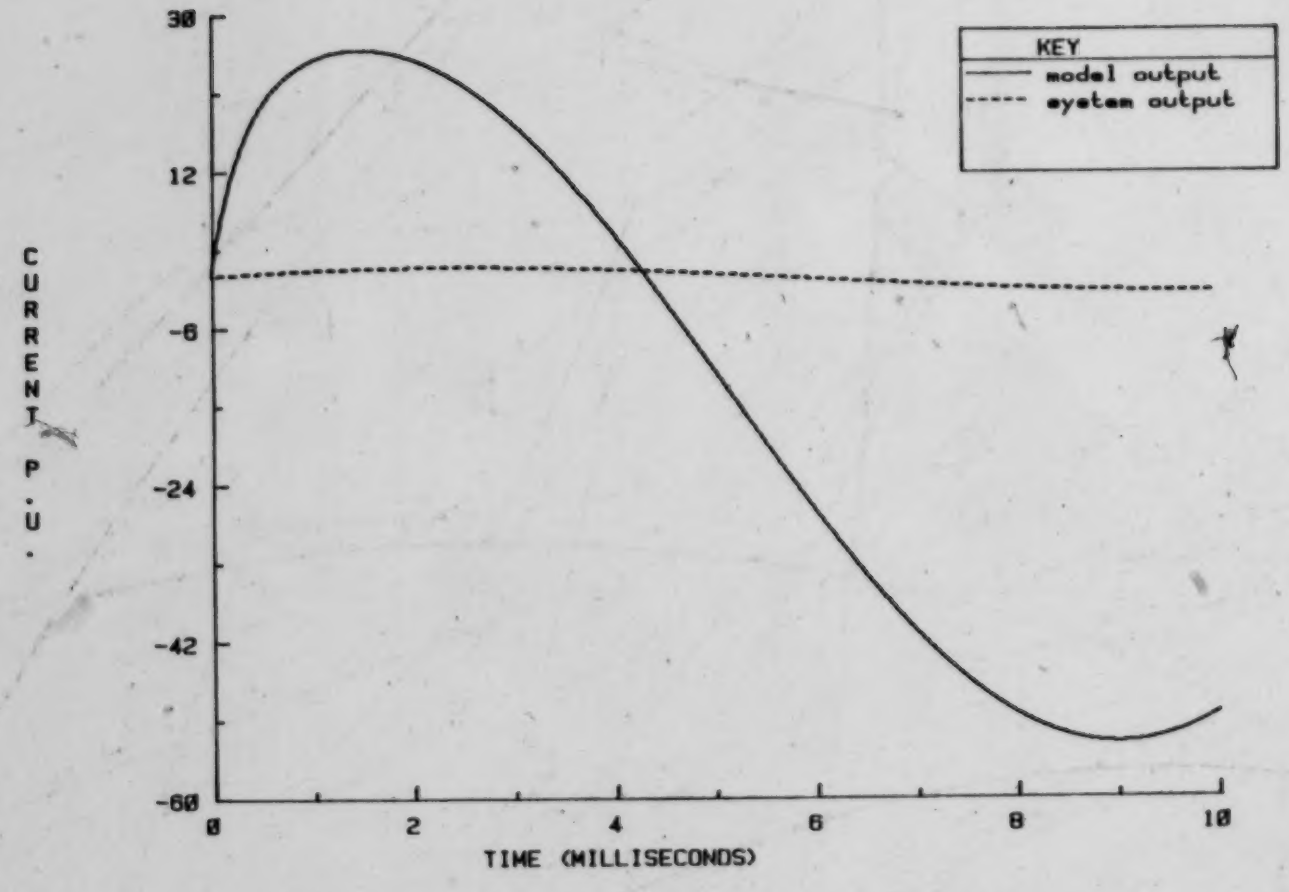

Figure 5.13 Output waveform from test 1 with initial estimates

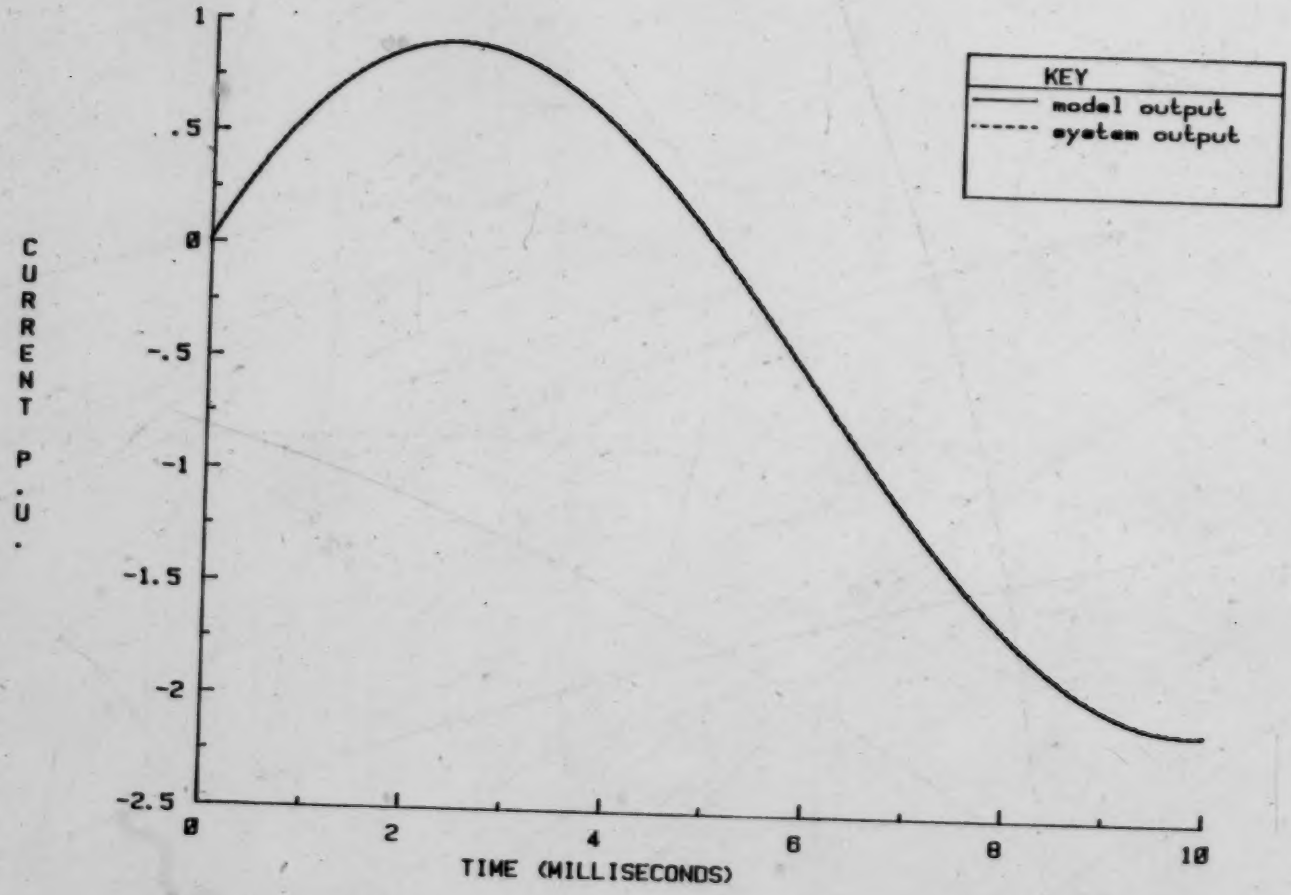

Figure 5.14 Output waveform from test 1 with identified parameters

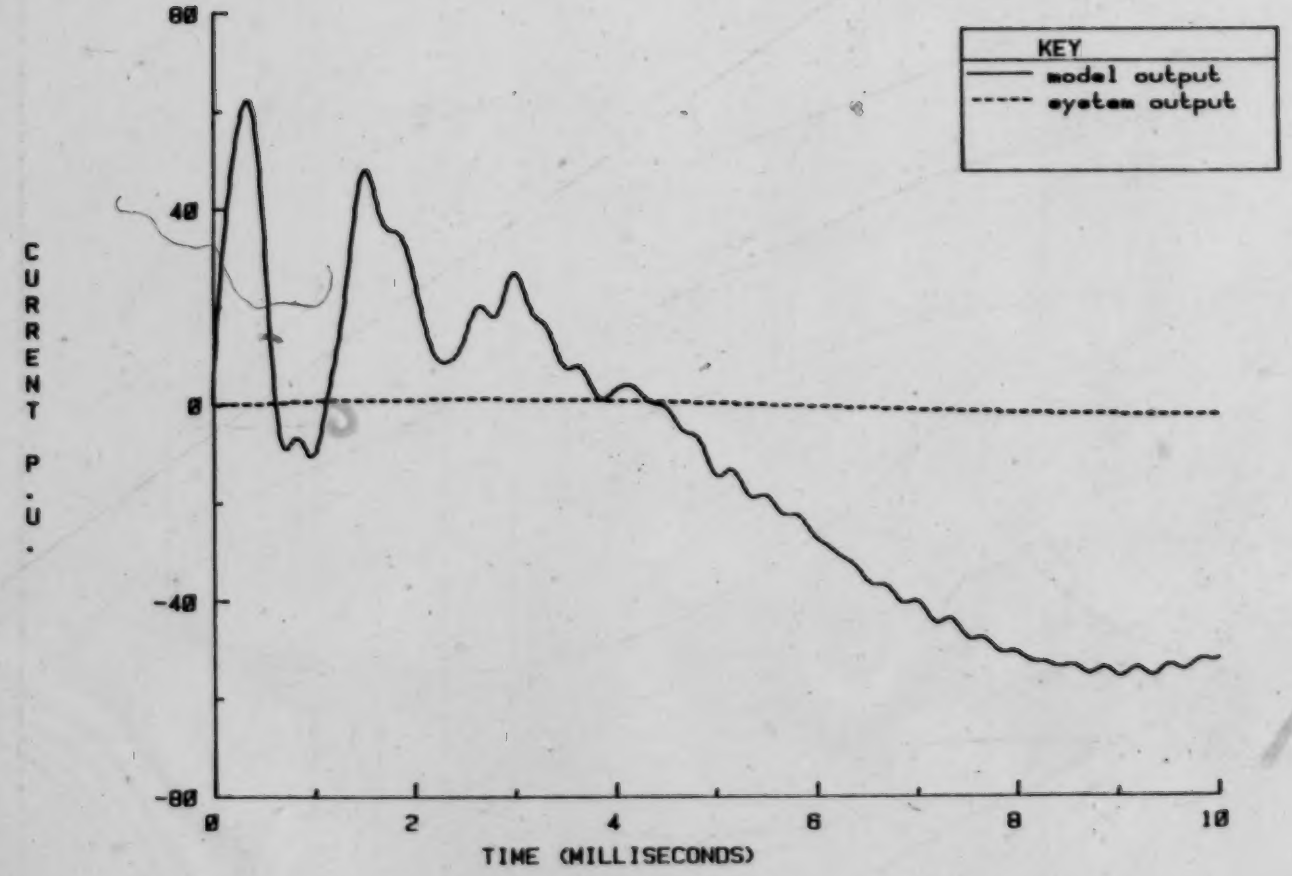

Figure 5.15 Output waveform from test 2 with initial estimates

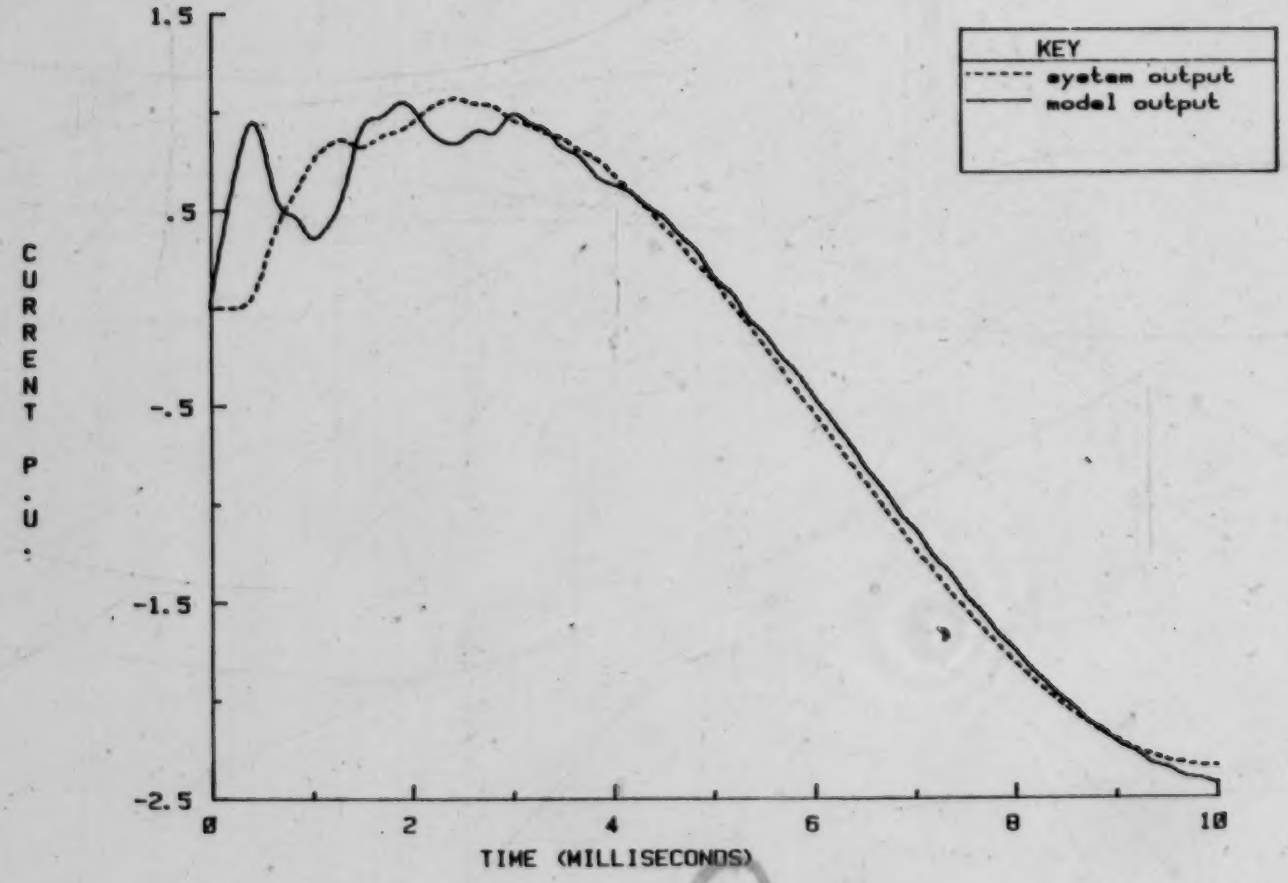

Figure 5.16 Output waveform from test 2 with identified parameters

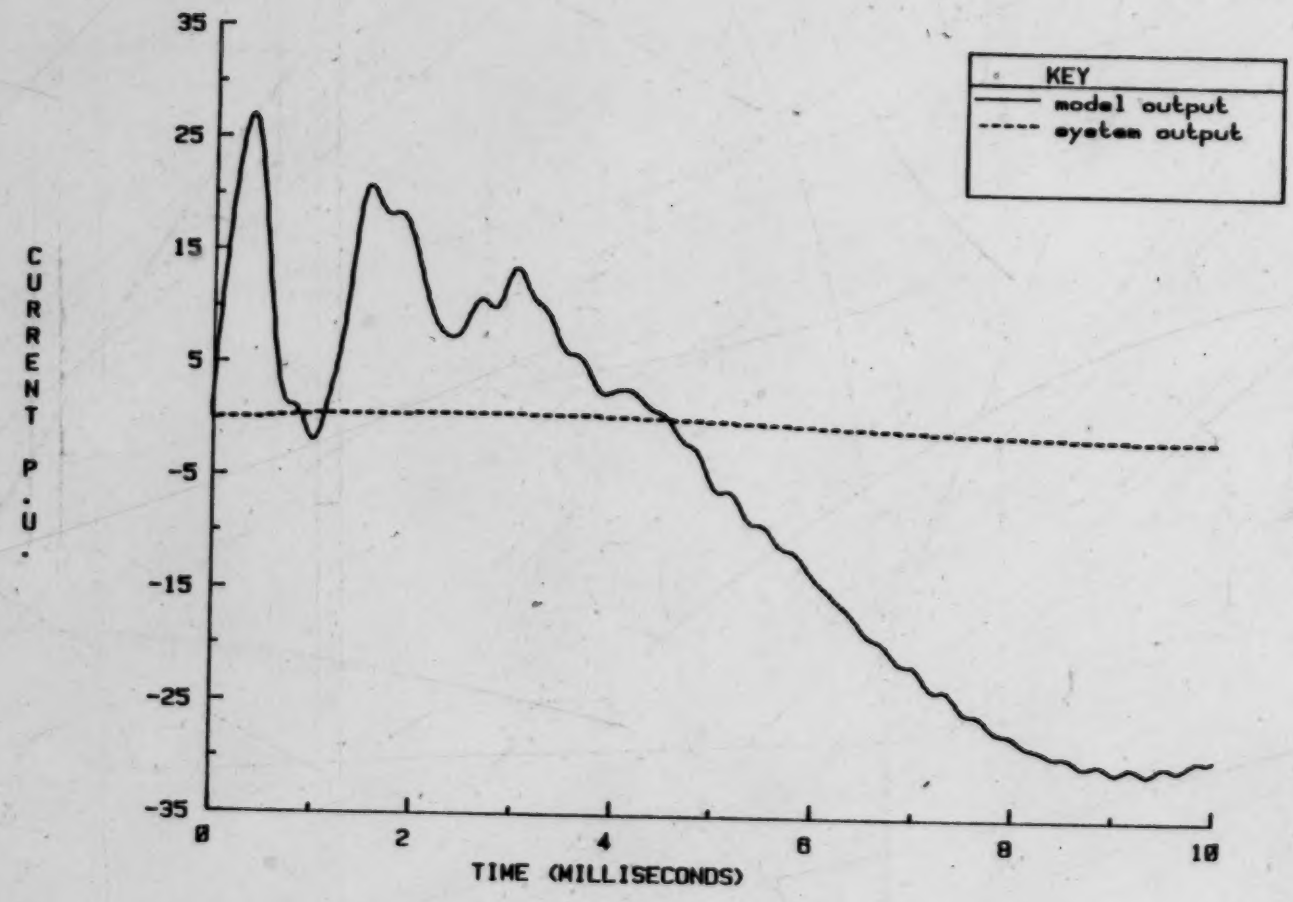

Figure 5.17 Output waveform from test 3 with initial estimates (positive sequence current)

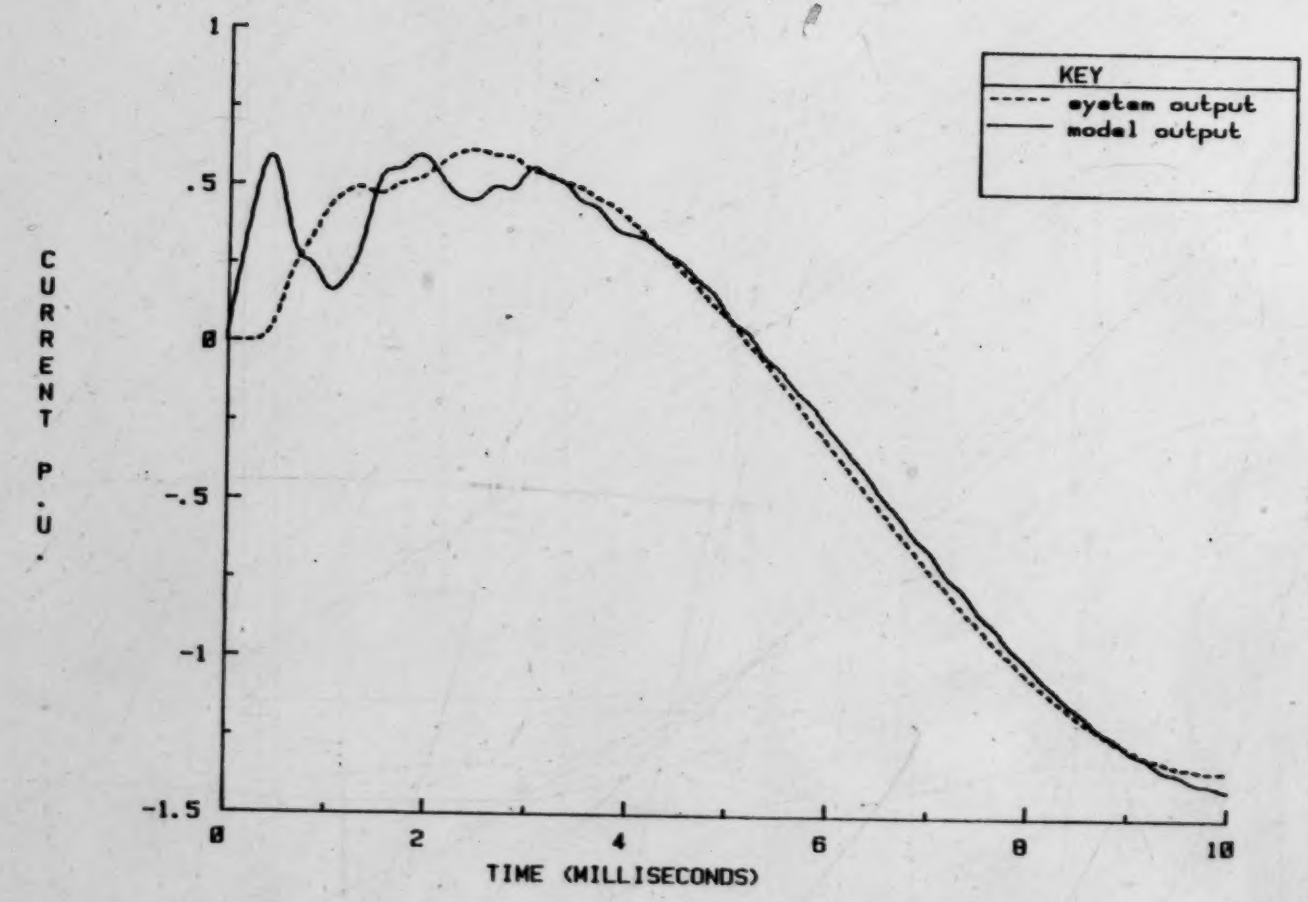

Figure 5.18 Output waveform from test 3 with identified parameters (positive sequence current)

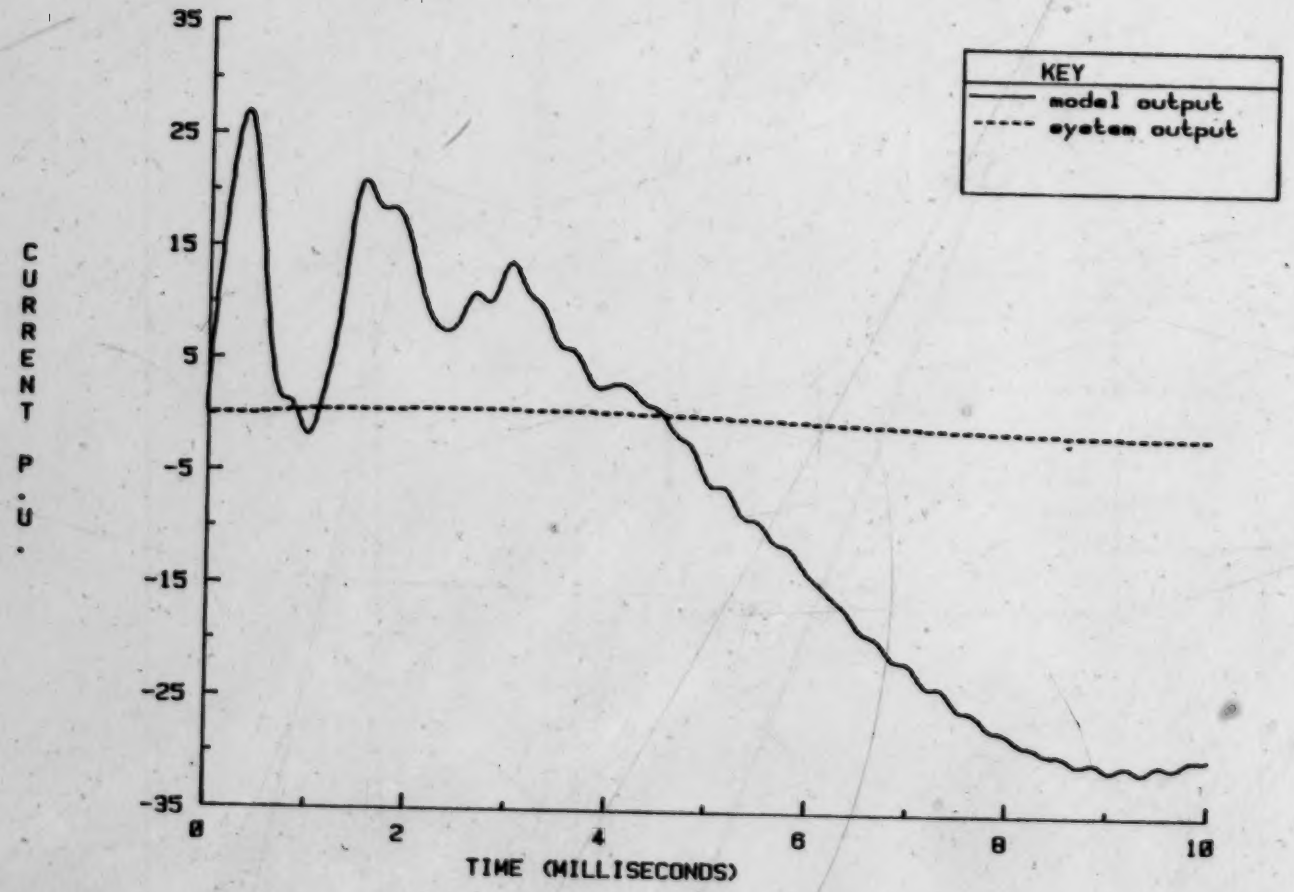

Figure 5.19 Output waveform from test 3 with initial estimates (zero sequence current)

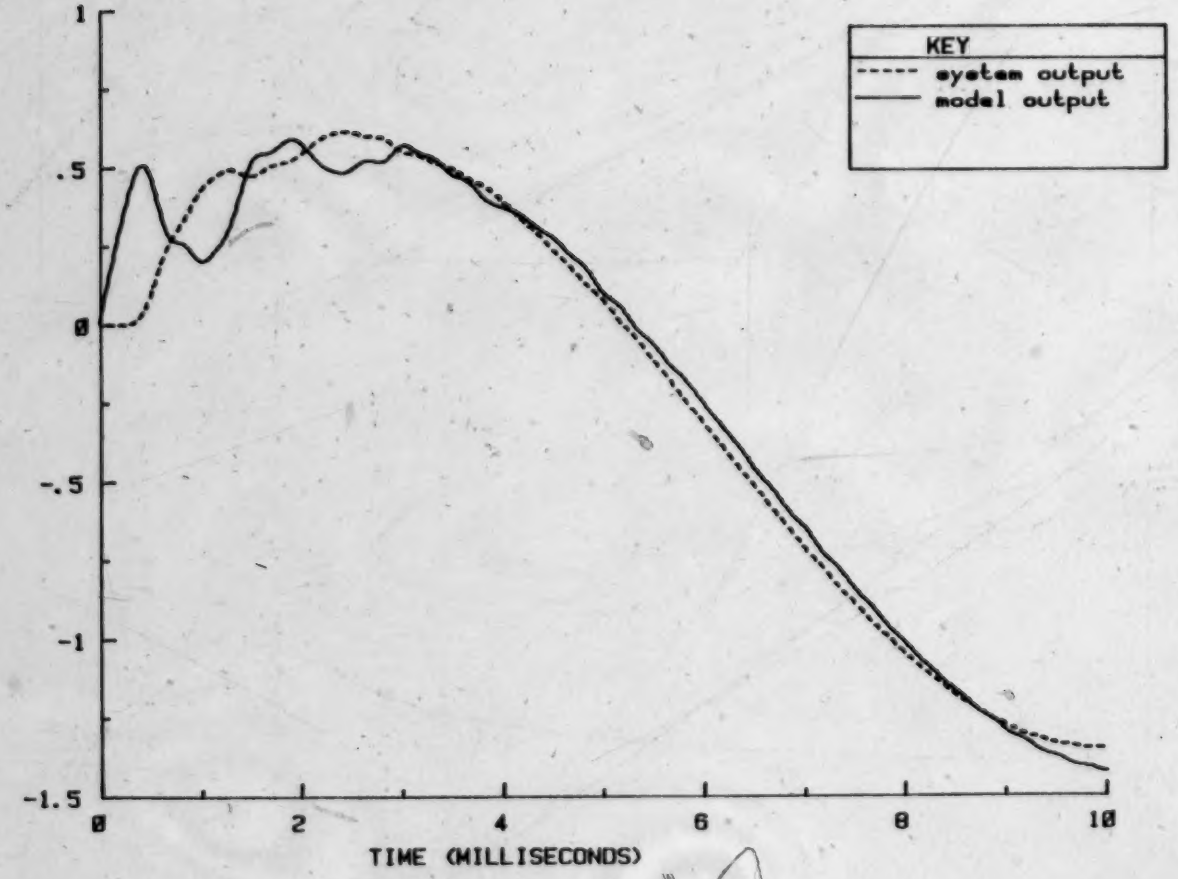

Figure 5.20 Output waveform from test 3 with identified parameters (zero sequence current)

CHAPTER VI

Conclusions

A parameter estimation fault location method using the least squares approach has been presented. No information about fault resistance is required *a priori* for the algorithm to estimate the fault location. The only information required is locally available voltages and currents. An attractive feature of this method is that filtering the fault data does not have to be performed before the algorithm is applied.

The simulation results show that fault location accuracy is relatively insensitive to fault resistance and fault distance.

For all cases, the parameter values of the chosen model were estimated with the same gain matrix G without difficulty of convergence.

Approximation errors inherent in the mathematical structure of the model do not appear to give any difficulty in identifying the parameters for the study of three phase fault. However, for the study of a single line to ground fault, this error is shown as a bias problem. This suggests that further work is required to choose the model so that it more closely represents the actual system.

Using industrial data to test this algorithm is a natural next step for future studies. It is a practical

exercise and is less prone to errors introduced due to simulating the real system. Furthermore, a better understanding of the modelling technique is essential to build a practical fault locator for application to on-site implementation.

References

[1] T. W. Stringfield, D. J. Marihart, R. F. Stevens, "Fault Location Methods for Overhead Lines", AIEE Trans., vol. 76, pp. 518-529, Aug. 1957.

[2] E. Born, J. Jager, "Fault Locators for High-Voltage Overhead Lines", Siemens Review, volume 33, pp. 487-91, Oct. 1966.

[3] A. P. Seethapathy, C. S. Sreenivansan, S. Jayaranman, "A New Device for Locating Faults on Unarmoured Power Cables", Irrigation & Power (India), vol. 23, pp. 487-9, Oct.1966.

[4] M. Vitins, "A Correlation Method for Transmission Line Protection", IEEE Trans. Power App. Syst., vol. PAS-97, pp. 1607-1615, Sept./Oct. 1978.

[5] J. Kohals, "Estimation of Fault Locations on Power Lines", Proceedings of the 3rd IFAC Symposium, pp. 393-402, Delft, the Netherlands, June 1973.

[6] A. W. Brooks, "Distance Relaying using Least-Squares Estimates of Voltage, Current and Impedance", IEEE Conf. Proc. Power Ind. Comput. Appl. Conf. PICA '77, 10th Toronto, Ont., pp. 394-402, May 24-27, 1977.

[7] M. S. Sachdev, M. A. Baribeau, "A New Algorithm for Digital Impedance Relays", IEEE Trans. Power App. Syst., vol. PAS-98, pp. 2232-2240, Nov./Dec. 1979.

[8] W. J. Smolinski, "An Algorithm for Digital Impedance Calculation Using a Single pi Section Transmission Line Model", IEEE Trans. Power App. Syst., vol. PAS-98, pp. 1546-1551, Sept./Oct. 1979.

[9] T. Takagi, Y. Yamakosai, J. Baba, K. Uemura & T. Sakaguchi, "A New Algorithm of an Accurate Fault Location for EHV/UHV Transmission Lines; Part I-Fourier Transformation Method", IEEE Trans. Power App. Syst., vol. PAS-100, pp. 1316-1323, March 1981.

[10] M. T. Sant & Y. G. Paithankar, "On Line Digital Fault Locator for Overhead Transmission Line", Proc. IEE, vol. 126, pp.1181-1185, Nov. 1979.

[11] G. G. Richards, O. T. Tan, "An Accurate Fault Location Estimator for Transmission Line", IEEE PES Summer Meeting, Portland, Oregon, Paper 81 SM 345-0, July, 1981.

[12] Y. H. Ku, "Electric Energy Conversion", New York: Ronald Press Company, pp. 141, 1959.

[13] W. V. Lyon, "Transient Analysis of Alternating Current Machinery", New York: John Wiley & Sons, Inc., pp. 28-42, 1954.

[14] J. H. Anderson, A. G. Heaton, "Transient Analysis of Power Line/Cable Systems", Proc. IEE, vol. 113, No.12, pp.2017-2022, Dec. 1966.

[15] R. Uram, R. W. Miller, "Mathematical Analysis and Solution of Transmission Line Transients I- Theory and II- Applications", IEEE Trans. Power App. Syst., vol. PAS-83, pp.1116-1137, 1964.

[16] A. Greenwood, "Electrical Transients in Power Systems", New York: Wiley-Interscience, 1971.

[17] W. D. Stevenson, "Element of Power System Analysis", New York: McGraw Hill, 3rd edition, 1975.

[18] P. M. Anderson, "Analysis of Faulted Power Systems", The Iowa State University Press, 1973.

[19] E. Clarke, "Circuit Analysis of A-C Power Systems", vol. 1, New York: John Wiley & Sons, Inc. 1943.

[20] C. F. Wagner , R. D. Evans, "Symmetrical Components" , New York: McGraw Hill, Inc. 1933.

[21] H. H. Skilling, "Electric Transmission Lines", New York: McGraw Hill, Inc. 1951.

[22] R. Deutsch, "System Analysis Techniques" ,New Jersey, Englewood Cliffs, Prentice-Hall, Inc., pp. 202-211, 1969.

[23] J. M. Mendel, "Discrete Techniques of Parameter Estimation", New York: Marcel Dekker, Inc., pp. 55-133, 1973.

[24] P. Eykhoff, "System Identification", New York: John Wiley & Sons, Inc., 1974.

[25] O. Wing, "Circuit Theory with Computer Methods", New York: Holt Rinehart and Winston, Inc., pp.434-472, 1972.

Appendix A1 : Circuit parameters for a transmission line

Table A1 : 500 KV Transmission line model parameters (in per unit values, 500 KV, 1000 MVA base)[11]

parameter	zero sequence	positive sequence
line resistance R/mile	$15.54*10^{-4}$	$1.31*10^{-4}$
line reactance $\omega_o L$/mile	$64.21*10^{-4}$	$21.67*10^{-4}$
line susceptance $\omega_o C$/mile	$1.15*10^{-3}$	$1.97*10^{-3}$
Thevenin resistance R_r	$70.0*10^{-4}$	$70.0*10^{-4}$
Thevenin reactance $\omega_o L_r$	0.249	0.349

Appendix A2 : Derivation of State Space Form for a R-L Series Transmission Line

A 2.1 steady state analysis

The following calculations are referred to Figure 3.1.

$V_s = 1.0 \angle 5°$ $V_r = 1.0 \angle 0°$

$$\text{total } Z = 2(70.0*10^{-4}+j0.349)+1.31*10^{-2}+j21.67*10^{-3}$$
$$= 0.0271+j0.9147$$
$$= .9151\angle 88.3°$$

$$\bar{I}_a = (\bar{V}_s-\bar{V}_r)/Z$$
$$= (0.996195+j0.087156-1)/(0.9151\angle 88.3°)$$
$$= (-0.003805+j0.087156)/(0.9151\angle 88.3°)$$
$$= (0.087239\angle 92.5°)/(0.9151\angle 88.3°)$$
$$= 0.095333\angle 4.2°$$
$$= 0.095077+j0.006980$$

$$\bar{V}_a = \bar{V}_s - \bar{I}_a(R_{r1}+j\omega L_{r1})$$
$$= 0.999421\angle 3.1°$$

A2.2 Initial condition calculation

$$v_s = 1.0\cos(377*t+5°)$$

$$v_r = 1.0\cos(377*t)$$

assume the instant of fault inception occurs at $t_f = 1.0337*10^{-3}$

$$v_s(t_f^+) = 0.888394$$

since current through an inductor cannot change instantaneously. Thus

$$\bar{I}_a(t_f^-) = \bar{I}_a(t_f^+)$$

$$\bar{I}_a = 0.095333\angle 4.2°$$

$$i_a(t) = 0.095333\cos(377*t+4.2°)$$

$$i_a(1.0337*10^{-3}) = 0.085297$$

assume the fault occurs at the middle of the line, the network can be drawn as :

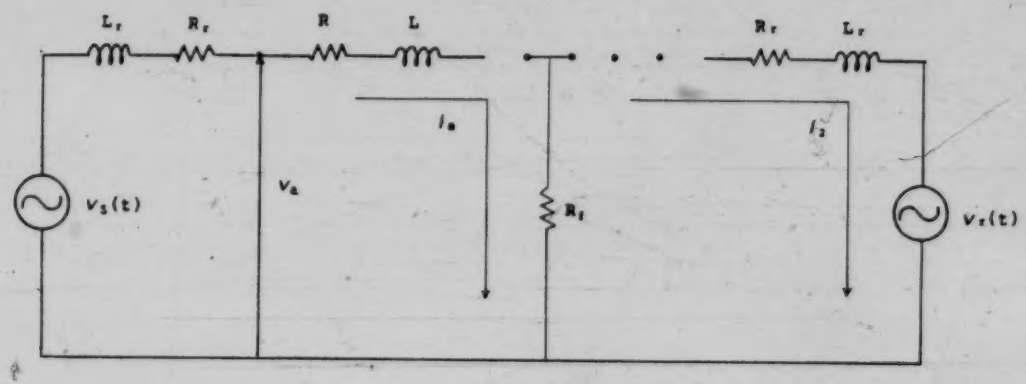

Note $i_2(t_f^+) = i_2(t_f^-)$

Also $i_2(t_f^-) = i_a(t_f^-)$

Therefore $i_a(t_f^+) = i_2(t_f^+)$.

Hence, the initial condition does not depend on the location of fault.

A2.3 state space model

Let the entire line be represented by eight sections and N be the number of sections or fault distance at which a fault occurs. Applying KVL to loop 1 :

$$-v_s + R_r i_a + L_r \dot{i}_a + (N*R) i_a + (N*L) \dot{i}_a + R_f(i_a - i_2) = 0 \qquad \text{(A2.1)}$$

Applying KVL to loop 2 :

$$-R_f(i_a - i_2) + (8-N)*R*i_2 + (8-N)*L*\dot{i}_2 + R_r i_2 + L_r \dot{i}_2 + v_r = 0 \qquad \text{(A2.2)}$$

Rearranging these equations so that they can be expressed in state space form of equation (4.1) :

$$\dot{X} = A\,X + B\,U \qquad \text{(A2.3)}$$

$$\dot{i}_a = \frac{-(R_r+N*R+R_f)}{L_r+N*L} i_a + \frac{R_f}{L_r+N*L} i_2 + \frac{1}{L_r+N*L} v_s \qquad \text{(A2.4)}$$

$$\dot{i}_2 = \frac{R_f}{L_r+(8-N)*L} i_a + \frac{-(R_r+(8-N)*R+R_f)}{L_r+(8-N)*L} i_2 - \frac{1}{L_r+(8-N)*L} v_r \qquad \text{(A2.5)}$$

where,

$$X = \begin{bmatrix} i_a \\ i_2 \end{bmatrix} \qquad \text{(A2.6)}$$

$$U = \begin{bmatrix} V_f \\ V_r \end{bmatrix} \tag{A2.7}$$

$$A = \begin{bmatrix} \dfrac{-(R_r+N*R+R_f)}{L_r+N*L} & \dfrac{R_f}{L_r+N*L} \\ \dfrac{R_f}{L_r+(8-N)*L} & \dfrac{-(R_r+(8-N)*R+R_f)}{L_r+(8-N)*L} \end{bmatrix} \tag{A2.8}$$

$$B = \begin{bmatrix} \dfrac{1}{L_r+N*L} & 0 \\ 0 & \dfrac{-1}{L_r+(8-N)*L} \end{bmatrix} \tag{A2.9}$$

Appendix A3 :Derivation of state space form for eight π sections transmission line

The following calculations are referred to Figure 3.2. Applying Kirchhoff's voltage law (KVL) to each loop and applying Kirchhoff's current law (KCL) to each node yields the following equations :

KVL

$$\text{loop 1:}\quad -v_s + R_r i_1 + L_r \dot{i}_1 + v_1 = 0$$

$$\dot{i}_1 = -i_1 \frac{R_r}{L_r} + \frac{v_s}{L_r} - \frac{v_1}{L_r}$$

$$\text{loop 2:}\quad -v_1 + R i_2 + L \dot{i}_2 + v_2 = 0$$

$$\dot{i}_2 = -i_2 \frac{R}{L} + \frac{v_1}{L} - \frac{v_2}{L}$$

$$\text{loop 3:}\quad -v_2 + R i_3 + L \dot{i}_3 + v_3 = 0$$

$$\dot{i}_3 = -i_3 \frac{R}{L} + \frac{v_2}{L} - \frac{v_3}{L}$$

$$\text{loop 4:}\quad -v_3 + R i_4 + L \dot{i}_4 + v_4 = 0$$

$$\dot{i}_4 = -i_4 \frac{R}{L} + \frac{v_3}{L} - \frac{v_4}{L}$$

loop 5: $-v_4 + Ri_5 + L\dot{i}_5 + v_5 = 0$

$$\dot{i}_5 = -i_5\frac{R}{L} + \frac{v_4}{L} - \frac{v_5}{L}$$

loop 6: $-v_5 + Ri_8 + L\dot{i}_8 + v_8 = 0$

$$\dot{i}_8 = -i_8\frac{R}{L} + \frac{v_5}{L} - \frac{v_8}{L}$$

loop 7: $-v_8 + Ri_7 + L\dot{i}_7 + v_7 = 0$

$$\dot{i}_7 = -i_7\frac{R}{L} + \frac{v_8}{L} - \frac{v_7}{L}$$

loop 8: $-v_7 + Ri_8 + L\dot{i}_8 + v_8 = 0$

$$\dot{i}_8 = -i_8\frac{R}{L} + \frac{v_7}{L} - \frac{v_8}{L}$$

loop 9: $-v_8 + Ri_9 + L\dot{i}_9 + v_9 = 0$

$$\dot{i}_9 = -i_9\frac{R}{L} + \frac{v_8}{L} - \frac{v_9}{L}$$

loop 10: $-v_9 + R_r i_{10} + L_r \dot{i}_{10} + v_r = 0$

$$\dot{i}_{10} = -i_{10}\frac{R_r}{L_r} + \frac{v_9}{L_r} - \frac{v_r}{L_r}$$

KCL

node 1: $-i_1 + i_2 + C_1\dot{v}_1 = 0$

$$\dot{v}_1 = \frac{i_1}{C_1} - \frac{i_2}{C_1}$$

nole 2: $-i_2 + i_3 + C_2\dot{v}_2 = 0$

$$\dot{v}_2 = \frac{i_2}{C_2} - \frac{i_3}{C_2}$$

node 3: $-i_3 + i_4 + C_2\dot{v}_3 = 0$

$$\dot{v}_3 = \frac{i_3}{C_2} - \frac{i_4}{C_2}$$

node 4: $-i_4 + i_5 + C_2\dot{v}_4 = 0$

$$\dot{v}_4 = \frac{i_4}{C_2} - \frac{i_5}{C_2}$$

node 5: $-i_5 + i_6 + C_2\dot{v}_5 = 0$

$$\dot{v}_5 = \frac{i_5}{C_2} - \frac{i_6}{C_2}$$

node 6: $-i_6 + i_7 + C_2\dot{v}_6 = 0$

$$\dot{v}_6 = \frac{i_6}{C_2} - \frac{i_7}{C_2}$$

node 7: $-i_7 + i_8 + C_2\dot{v}_7 = 0$

$$\dot{v}_7 = \frac{i_7}{C_2} - \frac{i_8}{C_2}$$

node 8: $-i_8 + i_9 + C_2\dot{v}_8 = 0$

$$\dot{v}_8 = \frac{i_8}{C_2} - \frac{i_9}{C_2}$$

node 9: $-i_9 + i_{10} + C_1\dot{v}_9 = 0$

$$\dot{v}_9 = \frac{i_9}{C_1} - \frac{i_{10}}{C_1}$$

These equations can be expressed in the form of equation (4.1), where A and B can be written as :

$$A = \begin{bmatrix} \frac{-R_r}{L_r} & & & & \frac{-1}{L_r} & & \\ & \frac{-R}{L} & & & \frac{1}{L} & \frac{-1}{L} & \\ & & \frac{-R}{L} & & & & \frac{1}{L} \quad \frac{-1}{L} \\ & & & \frac{-R_r}{L_r} & & & \frac{1}{L_r} \\ \frac{1}{C_1} & \frac{-1}{C_1} & & & & & \\ & \frac{1}{C_2} & \frac{-1}{C_2} & & & 0 & \\ & & \frac{1}{C_2} & \frac{-1}{C_2} & & & \\ & & & \frac{1}{C_1} & \frac{-1}{C_1} & & \end{bmatrix} \qquad \text{(A3.3)}$$

$$B = \begin{bmatrix} \frac{1}{Lr} & & & \\ & 0 & & 0 \\ & & 0 & \\ & & \frac{-1}{Lr} & \\ \hline 0 & & & 0 \end{bmatrix} \qquad \text{(A3.4)}$$

and U is the input vector of the form :

$$U = \begin{bmatrix} V_s \\ 0 \\ \vdots \\ 0 \\ V_r \\ \hline 0 \\ \vdots \\ 0 \end{bmatrix} \qquad \text{(A3.5)}$$

and X is a vector of the form:

$$X = \begin{bmatrix} j_1 \\ | \\ j_{10} \\ \hline V_1 \\ | \\ V_s \end{bmatrix} \qquad \text{(A3.6)}$$

A3.1 steady state analysis

The method of calculation is the same as in A2.1. Since the network solution requires a lot of computation, a digital computer program with the subroutine of 'LEQT1C' in IMSL library was used to determine the nodal voltages of the network in Figure 3.2. A program was written to calculate all the branch currents using these calculated voltages. The results are shown in Table A2.

Table A2 Steady state values of voltages and currents

nodal voltages

	original complex number	magnitude	angle(radian)
n1	.10723E+01 +j .55595E-01	.10737E+01	.51800E-01
n2	.10774E+01 +j .52911E-01	.10787E+01	.49070E-01
n3	.10810E+01 +j .50243E-01	.10822E+01	.46445E-01
n4	.10832E+01 +j .47595E-01	.10842E+01	.43911E-01
n5	.10840E+01 +j .44971E-01	.10849E+01	.41462E-01
n6	.10833E+01 +j .42375E-01	.10841E+01	.39097E-01
n7	.10812E+01 +j .39809E-01	.10819E+01	.36803E-01
n8	.10776E+01 +j .37277E-01	.10782E+01	.34579E-01
n9	.10725E+01 +j .34783E-01	.10731E+01	.32420E-01

branch currents

b1	.86035E-01 +j .21981E+00	.23605E+00	.11977E+01
b2	.87385E-01 +j .19357E+00	.21238E+00	.11467E+01
b3	.90132E-01 +j .13836E+00	.16513E+00	.99342E+00
b4	.92509E-01 +j .86815E-01	.12687E+00	.75366E+00
b5	.94742E-01 +j .35231E-01	.10108E+00	.35602E+00
b6	.97045E-01 +j-.19975E-01	.99079E-01	-.20300E+00
b7	.99055E-01 +j-.71538E-01	.12219E+00	-.62547E+00
b8	.10114E+00 +j-.12679E+00	.16219E+00	-.89746E+00
b9	.10308E+00 +j-.18202E+00	.20918E+00	-.10555E+01
b10	.10379E+00 +j-.20566E+00	.23037E+00	-.11034E+01

A3.2 Initial condition calculation

Current through an inductor and voltage across a capacitor cannot change instantaneously. Hence, at the instant of the fault, voltage and current will retain their prefault values. In other words,

$$i(t_f^-) = i(t_f^+)$$

and,

$$v(t_f^-) = v(t_f^+)$$

For instance, take branch current i_1, at the instant that the fault is assumed to occur at $t_f = 1.0337*10^{-3}$. Since prefault $i_1(t)$ can be expressed as :

$$i_1(t) = 0.23605*\cos(377*t+1.1977)$$

$$i_1(t_f) = -0.0039$$

Similarly, other initial conditions can be found by substituting the fault inception time in the corresponding prefault time functions.

Appendix A4 : Expression for equation (5.7)

After substituting equation (5.4) and equation (5.5) into equation (5.6), $\dot{I}_f$ becomes,

$$\dot{I}_f = \{\{[(d_o-d)R_o+R_{ro}] - \frac{(d_oR_o+R_{ro})[(d_o-d)L_o+L_{ro}]}{d_oL_o+L_{ro}}\}I_o$$

$$+ \{[2(d_o-d)R_1+2R_{r1}]$$

$$- \frac{(2d_oR_1+2R_{r1})[2(d_o-d)L_1+2L_{r1}]}{2d_oL_1+2L_{r1}}\}I_1$$

$$+ \{-[(d_o-d)R_o+R_{ro}]-[2(d_o-d)R_1+2R_{r1}]-3R_f$$

$$+ \frac{[(d_o-d)R_o+R_{ro}][(d_o-d)L_o+L_{ro}]}{d_oL_o+L_{ro}}$$

$$+ \frac{[2(d_o-d)R_1+2R_{r1}][2(d_o-d)L_1+2L_{r1}]}{2d_oL_1+2L_{r1}}\}I_f$$

$$+ \{\frac{(d_o-d)L_o+L_{ro}}{d_oL_o+L_{ro}}\}V_o + \{\frac{2[2(d_o-d)L_1+2L_{r1}]}{2d_oL_1+2L_{r1}}\}V_1$$

$$+ \sqrt{3}V_f\}/D$$

where,

$$D = [(d_o-d)L_o+L_{ro}] + [2(d_o-d)L_1+2L_{r1}]$$

$$- \frac{[(d_o-d)L_o+L_{ro}][(d_o-d)L_o+L_{ro}]}{d_oL_o+L_{ro}}$$

$$- \frac{[2(d_o-d)L_1+2L_{r1}][2(d_o-d)L_1+2L_{r1}]}{2d_oL_1+2L_{r1}}$$

Appendix A5 : Expression for equation (5.13)

After substituting equation (5.11) into equation (5.12), $\dot{I}_f$ becomes :

$$\dot{I}_f = \{[(d_o-d)R_1+R_{r1}]-\frac{[(d_o-d)L_1+L_{r1}][d_oR_1+R_{r1}]}{d_oL_1+L_{r1}}\}I_a$$

$$+ \{\frac{[(d_o-d)L_1+L_{r1}][(d_o-d)R_1+R_{r1}]}{d_oL_1+L_{r1}}-[(d_o-d)R_1+R_{r1}+R_f]\}I_f$$

$$+ \{\frac{[(d_o-d)L_1+L_{r1}]}{d_oL_1+L_{r1}}V_1+V_f\}/D$$

where

$$D = [(d_o-d)L_1+L_{r1}]-\frac{[(d_o-d)L_1+L_{r1}][(d_o-d)L_1+L_{r1}]}{d_oL_1+L_{r1}}$$

Appendix A6 : Verification of the Presence of Mutual Coupling in the Phase Quantities

Assume the tansmission line is balanced. The off diagonal terms of the sequence impedance matrix are zero. Z_{012} can be written as :

$$Z_{012} = \begin{bmatrix} Z_0 & 0 & 0 \\ 0 & Z_1 & 0 \\ 0 & 0 & Z_2 \end{bmatrix}$$

Let the phase impedance matrix be Z, and

$$Z = AZ_{012}A^{-1}$$

where

$$A = \begin{bmatrix} 1 & 1 & 1 \\ 1 & a^2 & a \\ 1 & a & a^2 \end{bmatrix}$$

$$A^{-1} = \begin{bmatrix} 1 & 1 & 1 \\ 1 & a & a^2 \\ 1 & a^2 & a \end{bmatrix}$$

$$Z = \begin{bmatrix} 1 & 1 & 1 \\ 1 & a^2 & a \\ 1 & a & a^2 \end{bmatrix} \begin{bmatrix} Z_0 & 0 & 0 \\ 0 & Z_1 & 0 \\ 0 & 0 & Z_2 \end{bmatrix} \begin{bmatrix} 1 & 1 & 1 \\ 1 & a & a^2 \\ 1 & a^2 & a \end{bmatrix}$$

$$Z = \begin{bmatrix} Z_0+Z_1+Z_2 & Z_0+aZ_1+a^2Z_2 & Z_0+a^2Z_1+aZ_2 \\ Z_0+a^2Z_1+aZ_2 & Z_0+Z_1+Z_2 & Z_0+aZ_1+a^2Z_2 \\ Z_0+aZ_1+a^2Z_2 & Z_0+a^2Z_1+aZ_2 & Z_0+Z_1+Z_2 \end{bmatrix}$$

The presence of the off diagonal terms indicates mutual coupling between phases.